https://doi.org/10.5194/egusphere-2026-1594
Preprint. Discussion started: 30 April 2026

Interferometric synthetic aperture radar (InSAR) phase data assimilation for Bayesian snow water equivalent estimation

Steven A. Margulis[1], Maya Hildebrand[1], Xiaolan Xu[2], Manuela Girotto[3], Hans-Peter Marshall[4], Rashmi Shah[2], Elias Deeb[5], Simon Yueh[2], Dara Entekhabi[6], Jessica Lundquist[7]

[1]Department of Civil & Environmental Engineering, University of California, Los Angeles, 90095, USA
[2]Jet Propulsion Laboratory, California Institute of Technology, Pasadena, 91109, USA
[3]Department of Environmental Science, Policy & Management, University of California, Berkeley, 94720, USA
[4]Department of Geosciences, Boise State University, Boise, 83725, USA
[5]Cold Regions Research and Engineering Laboratory, U.S. Army Corps of Engineers, Hanover, 03755, USA
[6]Department of Civil & Environmental Engineering, Massachusetts Institute of Technology, Cambridge, 02139, USA
[7]Department of Civil & Environmental Engineering, University of Washington, Seattle, 98195, USA

Correspondence to: Steven A. Margulis (margulis@seas.ucla.edu)

Abstract. Active microwave measurements, including those using interferometric synthetic aperture radar (InSAR) techniques, have shown promise for characterizing seasonal snowpacks at high spatial resolution. This study demonstrates a Bayesian InSAR phase data assimilation framework for estimating snow water equivalent (SWE) changes (dSWE) and SWE accumulation from dry-snow phase delay measurements at C-, L-, and P-band wavelengths. Two idealized synthetic end-member observing system simulation experiments (OSSEs) were performed in the context of a deep snow year at sites in the Tuolumne watershed. A baseline case with 6-day temporal repeat was used to evaluate the Bayesian framework relative to a deterministic retrieval approach under the two end-member cases where: (i) phase delay data is perfectly unwrapped and (ii) phase delay data is wrapped. In the case of perfectly unwrapped phase measurements, the deterministic retrieval and Bayesian approaches both show good estimation of dSWE across all three wavelengths (< 23 mm RMSE). The Bayesian approach shows reduced RMSE in dSWE (~63-74% of deterministic retrieval RMSE) and SWE (~5-34% of the deterministic retrieval RMSE). The primary source of error in SWE for the retrieval estimates is at the site where a month-long gap in measurements, due to wet snow early in the accumulation season, leads to missing dSWE events that result in SWE underestimation. In the case of fully wrapped phase measurements, ambiguity due to wrapping leads to very large (bias) errors in deterministically retrieved dSWE. The Bayesian framework uses an appropriate likelihood function to account for phase wrapping so that, when combined with the prior information provided by the modeling framework, results show minimal degradation to the perfectly unwrapped case in most test cases (except for the C-band case with a long temporal measurement gap). Tests examining the sensitivity to measurement error standard deviation and temporal repeat highlight the ability of the Bayesian approach to add value to the retrieval of dSWE and SWE across a range of cases. Future work should test the Bayesian framework with real InSAR phase data (e.g. Sentinel-1 C-band and NISAR L-band) across the range of physiographic and snow characteristics and phase retrieval error expected in mountain snow domains.

https://doi.org/10.5194/egusphere-2026-1594
Preprint. Discussion started: 30 April 2026

1 Introduction

Mountain ranges, where snow processes often dominate the water cycle, comprise nearly a quarter of the global land area (Wrzesien et al., 2019) and are hydrological hotspots due to orographic precipitation enhancement (Roe, 2005), with rainshadow and other effects that result in complex snow patterns over short geographic scales (Fang et al., 2023). Runoff from snow-covered mountains, provides a vital resource for downstream users, yet population growth and climate change have made many of these areas water stressed, leaving ecosystems, arable lands, and their dependent cities with insufficient water (Mankin et al., 2015; Qin et al., 2020; Immerzeel et al., 2020; Siirila-Woodburn et al., 2021). Managing water resources in these regions is difficult due to a lack of knowledge of the amount of snow water equivalent (SWE), stored upstream of where it is needed. Although satellites measuring in the visible through shortwave-infrared spectrum have successfully mapped snow cover *extent* for decades, progress in spaceborne measurement of mountain SWE has proved elusive. Consequently, management of water, energy, and food supply still often rely on sparse in situ measurements or models to estimate mountain SWE.

Passive microwave sensors have a long history of being used for estimating SWE for shallow snow over gentle terrain and under limited forest cover at tens of kilometer resolution (e.g., Chang et al., 1987), but are incapable of measuring the deep and variable snow characteristics of Earth's mountains (Metsämäki et al., 2015). Hence, many large-scale snow estimates based on these measurements mask out mountains altogether (Luojus et al., 2021). Estimating the spatial distribution of SWE in mountainous terrain is arguably the most important unsolved problem in snow hydrology (Dozier et al., 2016) and one "that is most in need of new strategic thinking from the hydrologic community" (Lettenmaier et al., 2015). Based on these arguments, mountain SWE has been designated by the U.S. National Academy of Sciences decadal survey of earth science priorities (NASEM, 2018) as among the "most important" targeted observables from space leading to several recent community-driven recommendations (Gascoin et al., 2024) and proposed SWE mission concepts (Hale et al., 2025).

Active microwave measurements are among these community-recommended solutions as they have the potential to sense SWE at spatial scales relevant in mountains. Ku-band (~15 GHz frequency, 0.02 m wavelength) can exploit volume scattering processes by snow to retrieve high spatial resolution SWE estimates (e.g., Yueh et al., 2009; Rott et al., 2010; Derksen et al., 2019; Tsang et al., 2022) over shallow to moderate snow depths (Garnaud et al., 2019; Takala et al., 2011; Rott et al., 2010). Measurements at C-band (~5 GHz, 0.06 m), L-band (~1.2GHz, 0.25 m), and P-band (~300 MHz, 1 m) have potential information on SWE change using interferometric phase delay that is less sensitive to snow grain size and snow stratigraphy. The shorter Ku- and C-band wavelengths are not conducive to penetrating forest canopies that often coincide with mountain snow. The longer L-band and P-band wavelengths could fill a crucial gap of deep mountain snow retrieval and snow under forest canopies (Jeong et al., 2023).

2 Background & Guiding Research Questions

2.1 InSAR remote sensing configurations for snow retrieval

In this paper we focus on demonstrating the feasibility of interferometric phase data assimilation as a Bayesian SWE estimation technique. This proof-of-concept is tested using observing system simulation experiments

https://doi.org/10.5194/egusphere-2026-1594
Preprint. Discussion started: 30 April 2026

(OSSEs) with synthetic measurements at C-, L-, or P-band frequencies. Study of these frequencies is motivated by InSAR mission platforms that already exist (Sentinel-1 at C-band; Nagler et al., 2015, and NISAR at L-band; Rosen et al., 2017), are planned for launch (ROSE-L at L-band; Davidson et al. 2022), or have been proposed as a potential mission concept (Signal of Opportunity (SoOp)-SAR at P-band; Yueh et al., 2021).

Figure 1 shows the basic geometry involved in either monostatic (backscattering) or bistatic (forward scattering) platforms. The former is representative of Sentinel-1, NISAR, and ROSE-L, while the latter is representative of a SoOp-SAR configuration (Yueh et al., 2021). Monostatic configurations have the transmitter (T_x) and receiver (R_x) on the same spacecraft. Hence the transmitter altitude H_T and receiver altitude H_R and the transmitter incidence angle θ_T and receiver incidence angle θ_R are the same (Fig. 1a). For a bistatic SoOp configuration, the transmitter (in geosynchronous orbit) and receivers (in low earth orbit) are on different spacecraft. Depending on receiver pointing, this may lead to different transmitter and receiver incidence angles, although when measuring in the desired specular plane (Yueh et al., 2021) they will be comparable (Fig. 1b).

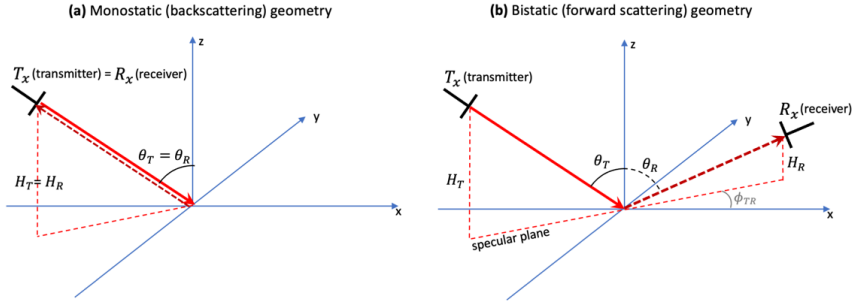

Figure 1. Geometry of (a) monostatic backscattering and (b) bistatic forward scattering InSAR configurations with a transmitter $\boldsymbol{T_x}$ and receiver $\boldsymbol{R_x}$. The transmitter incidence angle and receiver incidence angles are represented by $\boldsymbol{\theta_T}$ and $\boldsymbol{\theta_R}$ respectively. Both configurations rely on sufficient scattering of the transmitted radiation in the direction of the receiver.

Table 1 highlights the range of relevant baseline parameters for the C-, L-, and P-band mission platforms mentioned above. Despite frequency differences, many of the key parameters are similar, e.g., with temporal revisit in the range of 6-12 days, spatial resolution of tens to hundreds of meters, swath width of ~250 km, and incidence angles in the range of ~ 30-50°. The synthetic numerical experiments conducted herein, and described in more detail

Table 1. Baseline parameters for existing (Sentinal-1 and NISAR), planned (ROSE-L), and proposed (SoOp-SAR) InSAR missions examined in this study.

Mission/Concept	**Sentinel-1**	**NISAR**	**ROSE-L**	**SoOp-SAR**
Frequency	C-band (5.4 GHz)	L-band (1.25 GHz)	L-band (1.25 GHz)	P-band (370 MHz)
Configuration	Monostatic (constellation of 2 spacecraft)	Monostatic (1 spacecraft)	Monostatic (constellation of 2 independent spacecraft)	Bistatic (4 existing P-band transmitters with constellation of 3 spacecraft with receivers)
Temporal repeat	6-day (with both satellites)	12-day	6-day (with both satellites)	6-day
Spatial resolution	5 m x 20 m	3-48 m	<50 m^2	50-100 m
Swath	250 km	242 km	260 km	240 km
Incidence angle	29-40°	33-47°	29-46°	30-70°

https://doi.org/10.5194/egusphere-2026-1594
Preprint. Discussion started: 30 April 2026

below, focus on the footprint-scale (i.e., for a single InSAR footprint). A common incidence angle (40°) and common repeat frequency (6-day) is used for the baseline experimental setup to simplify intercomparison of results and focus on frequency-based differences. Sensitivity to temporal repeat is tested relative to the baseline case.

2.2 Physical basis of repeat-pass interferometry

2.2.1 Interferometric phase delay

The physical basis of repeat-pass (differential) interferometry for dry-snow SWE retrieval has been described in detail in Guneriussen et al. (2001), Rott et al. (2003), Deeb et al. (2011), Leinss et al. (2015), Li et al. (2017), Yueh et al. (2017), Conde et al. (2019), Nagler et al. (2022), Tarricone et al., (2024), Oveisgharan et al. (2024), Hoppinen et al. (2024), and references therein. The key aspects of interferometry involve the dielectric properties of snow (Text S1) and the impact of those properties on inducing a phase delay (ϕ_{snow}) in the reflected signal under SWE changes (due to refraction and reduced speed as the wave passes through snow). Most of the retrieval work cited above has focused on dry-snow conditions (i.e. where liquid water content (LWC) in the snowpack is zero), which is typically limited to parts of the snow accumulation season. Herein we focus only on assimilation of such dry-snow phase delay measurements and leave examination of potential assimilation of wet snow phase (e.g., Yueh et al., 2017) for future work.

A basic schematic of the refraction leading to phase delay for either monostatic or bistatic sensing is shown in Fig. 2. When snow is present, there will be scattering from both the air-snow and snow-soil interfaces (including multiple reflections within the snowpack). The difference in permittivity between air and snow at the air-snow interface causes a refraction of the beam and a reduction in the wave speed as it propagates through the snowpack. The signal is scattered from the rough snow-soil interface, where some fraction of power will be scattered in the direction of the receiver. For dry snow, an increase in SWE between two measurement times causes a phase delay (i.e., $\partial\phi_{snow}/\partial SWE > 0$ so that $\phi_{snow} > 0$).

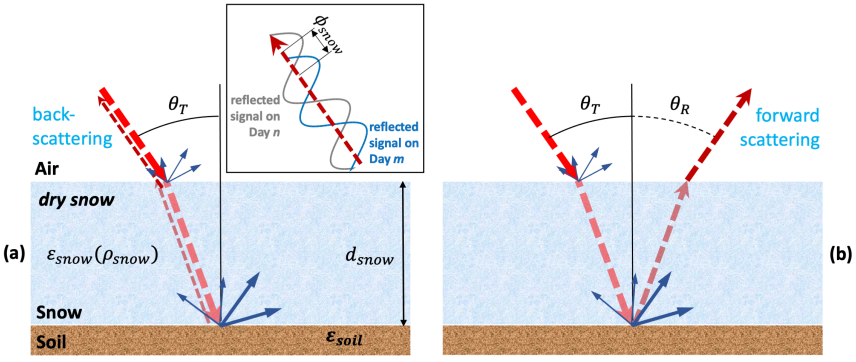

Figure 2. Illustration of scattering for dry-snow with (a) monostatic (backscattering) and (b) bistatic (forward scattering) measurement configurations respectively. Under dry-snow conditions, the bulk of the scattering occurs at the snow-soil interface. Inset shows a schematic representation of the phase delay between overpasses on two different days caused by SWE changes ($\boldsymbol{\phi_{snow}}$) that is expected in either monostatic or bistatic configurations.

https://doi.org/10.5194/egusphere-2026-1594
Preprint. Discussion started: 30 April 2026

To account for absorption and multiple reflections due to layering, the reflection coefficient for the bulk snowpack can be computed using a layered dielectric medium model as illustrated in Yueh et al. (2017) and described in more detail in Text S2. The phase delay can be computed as the angle of the complex reflection coefficient between two measurement times (t_{m1} and t_{m2}), i.e.:

$$\phi_{snow} = \angle(R_0)_{t_{m2}} - \angle(R_0)_{t_{m1}} \qquad (1)$$

where R_0 is the reflection coefficient at the air-snow interface, which, for dry snow, depends on the layered profiles of snow density and depth (Text S3). This layered model is difficult to apply in retrieval approaches due to the lack of a priori information on layering, but in the context of data assimilation can be useful, for diagnosing reflection source in dry vs. wet conditions or directly predicting phase delay, if the snow model provides a multi-layer representation of the snowpack (Sect. 3.3.1).

A first-order approximation of the multiple reflection model for phase delay described by Eq. (1) is the commonly used equation for dry-snow retrieval between two measurement times (Leinss et al., 2015):

$$\phi_{snow} = -2k_0[\{d_{snow,t_{m2}}\{\cos(\theta_T) - \sqrt{\varepsilon_{snow,t_{m2}} - \sin^2(\theta_T)}\} - \{d_{snow,t_{m1}}\{\cos(\theta_T) - \sqrt{\varepsilon_{snow,t_{m1}} - \sin^2(\theta_T)}\}] \qquad (2a)$$

$$\cong -2k_0\Delta d_{snow}\left[\cos(\theta_T) - I\sqrt{\varepsilon_{snow} - \sin^2(\theta_T)}\right] \qquad (2b)$$

where k_0 is the wavenumber ($2\pi/\lambda$), λ is wavelength, ε_{snow} is the (dry) snow permittivity, Δd_{snow} is the change in snow depth, and I is an indicator variable that equals 1 for dry snow. The approximate version of the equation assumes the permittivity (and hence density) of snow is relatively constant between overpasses. The snow density dependence of snow permittivity makes the phase delay a nearly linear function of *change* in SWE (dSWE) between two overpasses, making Eq. (2) a reliable basis for dSWE retrieval from measured ϕ_{snow}. Equation (2) can be applied for the monostatic and bistatic cases shown in Fig. 2. The first-order approximation given by Eq. (2) reasonably represents the phase delay in the layered model (Eq. (1)), where the primary difference is that the layered model accounts for reflection from the air-snow, internal snow, and snow-ground interfaces (Fig. S2a). C-band has the highest phase delay sensitivity to depth (SWE) changes, while P-band has the lowest sensitivity. Note that for sufficiently wet snow conditions, Yueh et al. (2017) provide a similar first-order approximation for the phase change associated with reflection from the air-snow interface (i.e., with $I = 0$ in Eq. (2b)) that closely approximates the layered model (Text S2).

2.2.2 Sources of error and ambiguity in interferometry

Many factors contribute to measured phase changes in an interferometric pair. In addition to snow effects, the total measured phase delay will be impacted by topography, the atmosphere (ionosphere and troposphere), spacecraft orbital position, terrain deformation, forest and soil moisture, and other effects (Wu and Madson, 2024; Text S3). To isolate the phase delay associated with snow, the first-order systematic impact of these other factors is typically removed from the total phase delay (Hoppinen et al., 2025). In deterministic retrieval algorithms, the observed value

https://doi.org/10.5194/egusphere-2026-1594
Preprint. Discussion started: 30 April 2026

of $\phi_{snow,obs}$ is then inverted to estimate dSWE using variants of Eq. (2), under the assumption of dry-snow. In a Bayesian data assimilation approach, the snow phase delay measurement uncertainty ($\sigma_{\phi_{snow}}$) is also a key parameter that could be derived in operational applications (Text S3). Deterministic retrieval approaches do not account for the phase delay measurement uncertainty explicitly. Nevertheless, such uncertainty is embedded in retrieved dSWE estimates as highlighted below. The measurement uncertainty in phase retrieval is expected to vary with frequency and in space and time (Text S3). Herein we investigate the impact of measurement error parametrically using constant values across different data assimilation experiments (Sect. 3.2).

Temporal decorrelation between pairs of measurements (i.e., when scattering properties change between measurement times) can limit the number of useful interferometric pairs for deriving phase delay for dSWE estimation (Text S4). There is a strong wavelength dependence on temporal correlation between measurements (Rott et al., 2003; Ruiz et al., 2022; Fig. S4). Ruiz et al. (2022) found sufficient temporal correlation for C- and L-band between 7 and 14 days. Because of its longer wavelength, P-band temporal correlation is most robust to between-scene sub-grid variations. The practical implication of this is that for a given repeat-frequency, fewer pairs of dry-snow measurements with sufficient correlation would be expected to be available at C-band compared to L- and P-band. Herein a simplified representation of synthetic measurement availability due to temporal decorrelation is used (Sect. 3.2).

Finally, the measured value of ϕ_{snow} is impacted by "phase wrapping" which limits values to a 2π range, i.e. $-\pi$ to π (-180° to 180°). Note that Eq. (2) predicts monotonically increasing phase delay with increasing dSWE, and thus represents an estimate of the "unwrapped" phase delay. The amount of SWE change corresponding to one phase wrapping cycle is a strong function of frequency (Text S5). When converted to dSWE, mapping across one ($-\pi$ to π) cycle at C-, L-, and P-band corresponds to approximately +/-20 mm, +/-60 mm, and +/-200 mm SWE change respectively. Phase wrapping thus leads to an increase in dSWE ambiguity at higher frequencies. Phase "unwrapping" algorithms (e.g., Goldstein et al., 1988; Fornaro et al., 1996; Ghiglia and Romero, 1996; Flynn, 1997; Costantini et al., 1999; Davidson and Bamler, 1999; Xu and Cumming, 1999; Chen and Zebker, 2000) are commonly applied to generate estimates of ϕ_{snow} that are integer multiples of π added to the measured (wrapped) values. The unwrapping process can introduce error in phase that propagates to dSWE retrieval (e.g., Oveisgharan et al., 2024; Hoppinen et al., 2024). In mountainous areas where SWE changes can be significant, phase wrapping is thus expected to impact the quality of retrieved dSWE estimates. In the data assimilation approach applied herein, the underlying Bayesian framework provides a natural way to use prior information to translate measured (wrapped) ϕ_{snow} to dSWE and to characterize its underlying uncertainty over the course of its seasonal evolution.

2.3 Research Questions

The rationale for this study is that a Bayesian data assimilation framework can be used to estimate dSWE (i.e., the amount of accumulated SWE in between overpasses) and total SWE (since the start of accumulation) from a sequence of repeat-pass pairwise phase delay measurements. This approach offers the potential for adding value to deterministic retrieval algorithm approaches, especially as related to the error and ambiguities described above. A Bayesian approach that models snow physics and phase delay can leverage that prior information to improve estimation. This study aims to answer the following questions in the context of deep mountain snow:

https://doi.org/10.5194/egusphere-2026-1594
Preprint. Discussion started: 30 April 2026

1. What is the projected performance of a Bayesian InSAR phase data assimilation approach for estimating dSWE and SWE?
2. How do dSWE and SWE estimates from a Bayesian approach compare to those using a deterministic retrieval approach?
3. How does performance compare across frequencies (C-, L-, and P-band), under measurement error, and with respect to ambiguities related to phase wrapping?

The questions are addressed in the context of idealized OSSEs applied to mountainous snow conditions that are chosen to challenge the limits of SWE estimation and retrieval.

3 Application Site, Experimental Design, and Methods

3.1 Application Site

In this study we use the upper Tuolumne River watershed in California as a representative testbed for assessing the proposed estimation method in an environment with deep mountain snowpacks where SWE changes throughout the season are significant and intermittent liquid water is expected in the snowpack. Three illustrative sites are chosen within the upper Tuolumne (Paradise Meadows (PDS), Tuolumne Meadows (TUM), and Dana Meadows (DAN); Fig. 3) that are relatively flat, in forest clearings, and have in situ data (snow pillows and courses) to ensure realistic representation of seasonal SWE dynamics. The sites are respectively at elevations of ~2356 m, ~2636 m, and ~2980 m (spanning approximately 300 m in elevation between sites). All sites are snow-dominated regimes with a distinct accumulation and ablation season spanning from earlier melt onset during the accumulation season at PDS to mostly dry snowpack throughout the accumulation season at DAN (Sect. 4.1). While the experimental framework is easily extendable to other water years, we limit the analysis here to a single (high-snow) year (Water Year (WY) 2017; Fang et al., 2022).

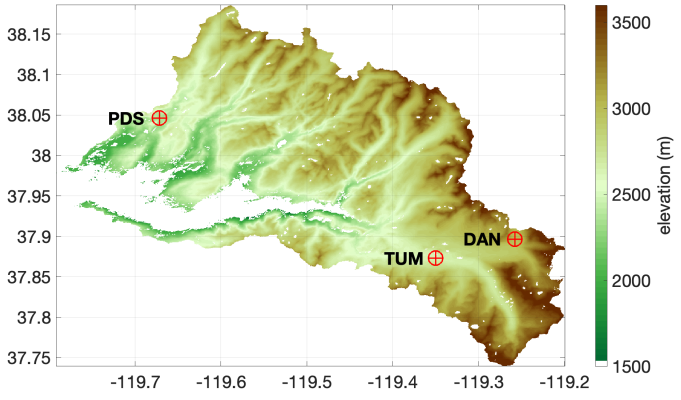

Figure 3. Upper Tuolumne watershed in the Sierra Nevada of California with digital elevation model (DEM). The OSSEs are performed at the Paradise Meadows (PDS), Tuolumne Meadows (TUM), and Dana Meadows (DAN) sites, which represent high-elevation locations that are relatively flat and in forest clearings.

https://doi.org/10.5194/egusphere-2026-1594
Preprint. Discussion started: 30 April 2026

3.2 OSSE Framework and Experimental Design

OSSEs (Masutani et al., 2010) are a commonly used tool for assessing the potential feasibility of new measurements and/or measurement configurations in estimating geophysical variables. Since no collocated seasonal mountain measurement datasets spanning C- through P-band exist, an OSSE provides the best approach to test the feasibility and efficacy of estimating SWE from interferometric observations at different wavelengths. Previous OSSE examples in the context of snow state estimation from remote sensing measurements include, e.g., Durand and Margulis (2006, 2007); DeLannoy et al. (2010); Garnaud et al. (2019); Cho et al. (2022). An OSSE framework uses system models to generate true (i.e., "nature run") geophysical states, from which measurements can be synthesized using physically-based measurement models combined with expected measurement error and spatiotemporal sampling characteristics. In OSSEs, a Bayesian data assimilation method then often uses the synthetic measurements as inputs to assess how well the geophysical variables can be estimated.

The OSSE framework applied herein (Fig. 4) uses a community-based snow model (Sect. 3.3.1) with prescribed inputs to generate nature run (true) snow states. With the true snow states and the measurement model (Sect. 3.3.2), synthetic phase delay measurements are generated at a specified temporal repeat frequency and corrupted with measurement errors of prescribed statistics. The data assimilation framework (Sect. 3.3.3) uses the synthetic measurements and a priori snow estimates to derive a posterior (Bayesian) estimate of the underlying snow states. Note that the proposed algorithm is a phase data assimilation framework rather than one that first retrieves dSWE and then assimilates the retrieved dSWE into the snow model (i.e., Shrestha and Barros, 2025). This is an important distinction that more fully accounts for the prior information (and uncertainty) provided by the modeling system and measurement process while avoiding assumptions about phase wrapping and snow wetness state used in deterministic retrievals. The posterior snow state estimates can then be compared to the true estimates as well as those that would be made by a traditional retrieval algorithm (i.e., via inversion of Eq. (2)) or a model-only (open loop) approach.

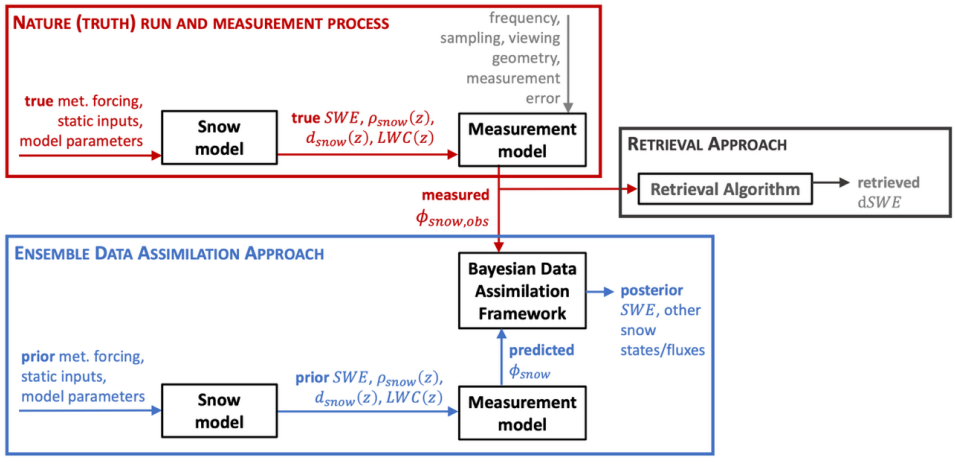

Figure 4. OSSE framework schematic showing generation of synthetic measurements using the snow and measurement models (red box), the ensemble data assimilation framework, which conditions prior snow states on the synthetic measurements (blue box), and a retrieval algorithm which uses phase measurements to derive dSWE estimates (grey box). The true snow states can be compared to the retrieval and posterior Bayesian (data assimilation) estimates. An open-loop (model-only) estimate consists of the prior estimates in the blue box.

https://doi.org/10.5194/egusphere-2026-1594
Preprint. Discussion started: 30 April 2026

All OSSEs performed in this study represent point-scale experiments using meteorological inputs and other characteristics corresponding to the PDS, TUM, or DAN sites, which are meant to mimic one InSAR measurement footprint, for WY 2017. We choose common baseline parameters to facilitate comparison across the three measurement frequencies (C-, L-, and P-band, Table 1): a 6-day temporal repeat, at a viewing angle of 40°, with a nominal phase measurement error of $\sigma_{\phi_{snow}}$ = 20°.

Two experiments are performed in this study to represent the end-member cases that bound dSWE and SWE estimation errors. Experiment #1 corresponds to the optimistic case where phase delay related to snow change is perfectly unwrapped (i.e., where dSWE values that go beyond the phase delay range of -180° to 180° are correctly unwrapped). This corresponds to the case with maximum possible signal-to-noise ratio, since phase is unbounded when unwrapped. Errors in dSWE estimation in Experiment #1 are impacted primarily by random phase measurement error of the specified characteristics. Experiment #2 corresponds to the pessimistic case with phase measurements that remain wrapped (i.e., exclusively within the measurable limits of -180° to 180°) with no knowledge whether some values require unwrapping. Hence additional errors in dSWE estimation (relative to Experiment #1) are expected due to the wrapping ambiguity. The wrapped phase not only adds ambiguity, but significantly reduces the signal-to-noise ratio since phase is bounded over a smaller range. The data assimilation framework can account for phase wrapping ambiguity by either assimilating unwrapped (Experiment #1) or wrapped data (Experiment #2) using different likelihood models (Sect. 3.3.3).

In practice, temporal repeat may be less frequent (e.g., 12-day for NISAR) and the measurement error is expected to vary with frequency and throughout the snow season (Eq. (S10)). Additional sensitivity experiments are performed to identify the impact of bulk measurement error and degraded temporal revisit frequency.

3.3 Modeling and Data Assimilation Framework

3.3.1 Snow Model

The snow model used herein is the Flexible Snow Model (FSM2), which is a modular multi-parameterization extension of the Factorial Snow Model (FSM; Essery, 2015). FSM2 is chosen for its parameterization options that span what is used by many community snow models (Essery et al., 2013) and for its application and testing across many studies (e.g., Magnusson et al., 2015; Krinner et al., 2018; Alonso-Gonzalez et al., 2018; 2021; Guenther et al., 2019; Mazzotti et al., 2020a, b; 2021; 2023; Pritchard et al., 2020; Mott et al., 2023). The FSM2 configuration represents the snowpack mass and energy balance with up to 3 snow layers. Dynamic (hourly) meteorological inputs include near-surface values of: precipitation, downwelling shortwave and longwave radiation, air temperature and humidity, wind speed, and atmospheric pressure. For the forest-free domains simulated herein there is no need for forest canopy parameterizations, so only snow parameterizations are used. Details of the FSM2 model setup are described in Text S6.

Meteorological model forcing inputs (and their uncertainties) follow what was done in Margulis et al. (2019), where a large-scale coarse-gridded (~ 50-100 km) reanalysis dataset (MERRA2; Gelaro et al., 2017) is downscaled to the modeling grid-cell using topographic corrections (Girotto et al., 2014). The DEM used in this work is the SRTM product available at 30 m resolution (Farr et al., 2007; NASA, 2013). Rather than downscaling precipitation, it is

https://doi.org/10.5194/egusphere-2026-1594
Preprint. Discussion started: 30 April 2026

modeled with large a priori uncertainty (and bias correction) that can be reduced via assimilation of measurements (Margulis et al., 2019). Uncertainty in precipitation and other meteorological inputs is discussed in Sect. 3.3.3.

3.3.2 Measurement Model

The measurement model uses modeled snow states as inputs to calculate phase delay between prescribed measurement times (e.g., with 6-day separation) for both generating synthetic phase delay measurements and for generating prior (ensemble) predicted phase delay (Fig. 4). When the snowpack is dry at both measurement times, Eq. (2) (with $I = 1$) is used to predict the phase delay. In the more complicated case where one or both pairwise snow states have non-zero LWC profiles within the snowpack, the multi-layer phase measurement model formulation (Text S2) is used as a diagnostic indicator to identify whether the snowpack behaves like: (i) a "dry snowpack" (i.e., with $I = 1$ in Eq. (2b)), (ii) a "sufficiently wet" snowpack (i.e., with $I = 0$ in Eq. (2b)), or (iii) an ambiguously wet snowpack (following neither first-order approximation). Hence, each measurement pair can be classified as a dry-dry, wet-wet, or mixed (dry-wet, wet-dry, or ambiguously wet) pair. Typically, shorter wavelengths (C-band) quickly transition between dry and sufficiently wet snowpacks, while longer wavelengths (P-band) can behave like a dry snowpack for larger amounts of LWC, but also have an ambiguous response for a larger range of LWC values.

Rather than attempting to simulate temporal coherence/decorrelation we use an idealized and simplified model: we assume temporal decorrelation occurs between any measurement pairs with more than 12 days of separation. Hence, under this simplified representation, only dry-dry pairs within a 12-day window are used to generate phase delay measurements. This simplified treatment ignores the expected frequency-dependence of temporal decorrelation (Text S4), potentially overestimating the number of available coherent pairs at C-band and underestimating the number of coherent pairs at P-band. Finally, the "measured" phase delay ($\phi_{snow,obs}$) is then generated by corrupting the true phase with random errors with zero-mean and prescribed measurement error standard deviation ($\sigma_{\phi_{snow}}$). For the prior ensemble predictions used in the assimilation framework, dry-dry realizations use Eq. (2b) with $I = 1$, wet-wet snowpack realizations use Eq. (2b) with $I = 0$, and mixed pairs are assumed to not yield a viable phase delay prediction (Sect. 3.3.3). In the case of Experiment #1, the phase is perfectly unwrapped, while in Experiment #2 the phase is in its wrapped state.

3.3.3 Bayesian Data Assimilation Approach

This study focuses on demonstrating the use of Bayesian data assimilation (DA) to generate dSWE and SWE estimates from phase delay observations, rather than on optimizing or comparing different assimilation methodologies, which we leave for future work. Herein we choose to apply a sequential particle filter (e.g., Liu and West, 2001; Arulampalam et al., 2002; Moradkhani et al., 2005) as a representative example to demonstrate how SWE estimation progresses throughout the snow season as measurements become available. Ensemble (particle) methods are useful in how they allow for representing the uncertainty of inputs and updating estimates from a discrete estimate of the prior probability density function (PDF) to a posterior PDF. The three key components of the DA framework are:
(i) the forward (snow) model:

$$\boldsymbol{x}_{i,t+1} = \boldsymbol{A}[\boldsymbol{u}_{i,t}, \boldsymbol{\beta}_{i,t}, \boldsymbol{x}_{i,t}] \qquad (3)$$

https://doi.org/10.5194/egusphere-2026-1594
Preprint. Discussion started: 30 April 2026

(ii) the measurement model:

$$y_{i,t} = M\left[\boldsymbol{x}_{i,t}\right] = M_{i,t} \qquad (4)$$

(iii) the likelihood function of the measurements given the states (at time t):

$$p_{y|\boldsymbol{x}} = p_v[Y_{obs} - M_{i,t}] \qquad (5)$$

In Eq. (3), $\boldsymbol{x}$ represents the snow state vector (multi-layer SWE, density, depth, LWC, etc.), $\boldsymbol{A}$ represents the FSM2 set of physical/empirical parameterizations (Sect. 3.3.1), $\boldsymbol{u}$ represents the meteorological forcing input vector (precipitation, air temperature, etc.; Sect. 3.3.1), $\boldsymbol{\beta}$ represents a parameter vector, and i (=1, …, N, where N is the ensemble size) and t represent indices for particle number and time respectively. Eq. (3) provides a prior estimate over the integration window (between measurements), where the prior weight of each particle is given by $w^{(i)} = 1/N$. In Eq. (4), y represents the predicted measurement (i.e., ϕ_{snow}) and $\boldsymbol{M}$ the mapping of snow states to phase delay with the added temporal constraint of the decorrelation time scale.

The likelihood function (Eq. (5)) is the conditional probability density function (PDF) of observations given the states, which is equivalent to the measurement error (v) PDF (p_v; Margulis et al., 2015). It is assumed that the measurement errors in phase delay are Gaussian and additive (as implicit in Eqs. (S11) and (S12)) with zero mean error and $\sigma_v = \sigma_{\phi_{snow}}$ measurement error standard deviation. For Experiment #1, where $\phi_{snow,obs}$ is perfectly unwrapped (unbounded), the typical Gaussian PDF is used for p_v. In Experiment #2, where $\phi_{snow,obs}$ is wrapped (bounded between -180° and 180°), we instead propose using the wrapped Gaussian PDF (Text S6; Agiomyrgiannakis and Stylianou, 2009; Kumar et al., 2022). The wrapped Gaussian PDF accounts for the fact that phase delay observations that are 2π different are equally likely, and provides a more natural way to assimilate unwrapped phase delay.

The primary source of modeled SWE uncertainty in the OSSEs is hypothesized to be the meteorological forcing (i.e., precipitation in particular). A priori precipitation is represented using the multiplicative bias-correction and uncertainty model in Margulis et al. (2019):

$$P_{i,t} = b_i P_{MERRA2,t} \qquad (6)$$

where $P_{MERRA2,t}$ represents the nominal MERRA2 precipitation and uncertainty is represented via lognormally distributed (seasonally-constant) multiplicative bias correction factors b_i using the same prescribed prior statistics (mean of 1.8 and coefficient of variation of 0.69) derived for the Western U.S. snow reanalysis (Fang et al., 2023). Additionally, uncertainty in air temperature is included using previously derived parameters (Fang et al., 2022). The true (nature run) precipitation multiplicative factor that scales MERRA2 precipitation (b_{true}) is independently derived for each station by fitting modeled SWE to that measured in situ at the PDS, TUM, and DAN sites with snow pillows and snow courses for WY 2017 (Sect. 4.1). Otherwise, all other nominal (downscaled) forcings are used in the nature run. Hence the true snow states are a single realization of the FSM2 model output forced by downscaled and bias-corrected meteorological forcings, while the a priori forcing is the same ensemble-based approach used in Margulis et al., (2019) and Fang et al. (2023).

https://doi.org/10.5194/egusphere-2026-1594
Preprint. Discussion started: 30 April 2026

Through the comparison of predicted a priori phase delay and observed phase delay, a sequential posterior estimate can be derived for both SWE (or more specifically dSWE since that is the variable that is related to the measured phase delay). The version of the particle filter used herein is that described by Liu and West (2001) with systematic resampling (Kuptametee and Aunsri, 2022), which allows for the derivation of posterior estimates for both snow states ($\boldsymbol{x}$) and parameters (in this case, the precipitation bias correction factor b). In this sequential application, the precipitation bias correction factor b is initially characterized by the prior distribution described above, with estimates of both snow states and b updated to posterior estimates with each phase measurement throughout the season (Text S7). The results herein are for an ensemble size of N=500.

The errors in the posterior Bayesian estimates for dSWE and SWE are computed relative to the true states. Two additional reference estimates are used for comparison: (1) deterministically retrieved dSWE and (2) a deterministic snow model estimate. The retrieved dSWE is obtained by simply inverting Eq. (2) as done in previous work (e.g., Oveisgharan et al., 2024; Hoppinen et al., 2024), herein using a lookup table between ϕ_{snow} and dSWE. As suggested by Oveisgharan et al., (2024), retrieval-based estimates of SWE during the accumulation season can be obtained from the retrieved dSWE values as: $SWE(t) = \sum_0^t dSWE$. Together these two additional references represent useful comparisons for the posterior Bayesian estimates: a no-measurement case (open loop model estimate only) and an only-measurement case (retrieval with no prior information).

4 Results and Discussion

4.1 OSSE true snow states and phase delay

The true (nature run) snow states are generated with FSM2, but with precipitation bias correction adjusted to fit in situ data at PDS, TUM and DAN in WY 2017. The calibrated WY 2017 bias corrections for MERRA2 were found to be 1.43, 1.14, and 1.63 for PDS, TUM, and DAN respectively (compared to the a priori mean bias correction of 1.8; Fang et al., 2022). Figure 5 shows a subset of the true snow states including SWE, snow depth, snow density, and LWC, the latter three of which are the required variables needed to predict phase delay (Eq. (2)). The SWE time series additionally shows the in situ snow pillow (daily) and snow course (monthly) data that was used to adjust precipitation for the nature run. Note that the snow pillow and course data is in close agreement at PDS. In contrast, substantial differences exist at TUM and DAN, illustrating the role of spatial representativeness when comparing point scale snow measurements (pillows) with those obtained across longer transects (courses). The (calibrated) true SWE captures the observed accumulation season (early December through mid-April), peak SWE (in mid-April), and ablation season (mid-April through late June) dynamics. Given that snow ablation is predicted reasonably well, no other downscaled forcings or parameters were adjusted in generating the true (nature run) states.

WY 2017 was a high snow year. PDS has the largest peak SWE (~2000 mm) while TUM is lowest (~1300 mm) and DAN (~1500 mm) is in between. The snow depth similarly varies across sites, from a peak of ~5000 mm in PDS to ~3800 mm at TUM. Snow density increases seasonally (with intermittent dips from snowfall) from ~200 kg m^{-3} in December to ~500 kg m^{-3} in June. FSM2 represents the snowpack with up to three layers, where the LWC in each layer (and in the bulk of the snowpack) is shown in the bottom panel of Fig. 5. Importantly, melt initiated in mid-

https://doi.org/10.5194/egusphere-2026-1594
Preprint. Discussion started: 30 April 2026

March near the snowpack surface leads to significantly higher LWC values (LWC~5-6%) in layer 1 (top 100 mm) and layer 2 (next 200 mm) than in the bulk of the snowpack (LWC<2%). This has important implications on phase delay, where a very wet near-surface snowpack will cause the snowpack to behave as sufficiently wet (Text S2), even when the bulk snowpack LWC is much smaller. It is for this reason that the multi-layer model is used in the measurement model to diagnose the behavior of the snowpack with respect to phase change.

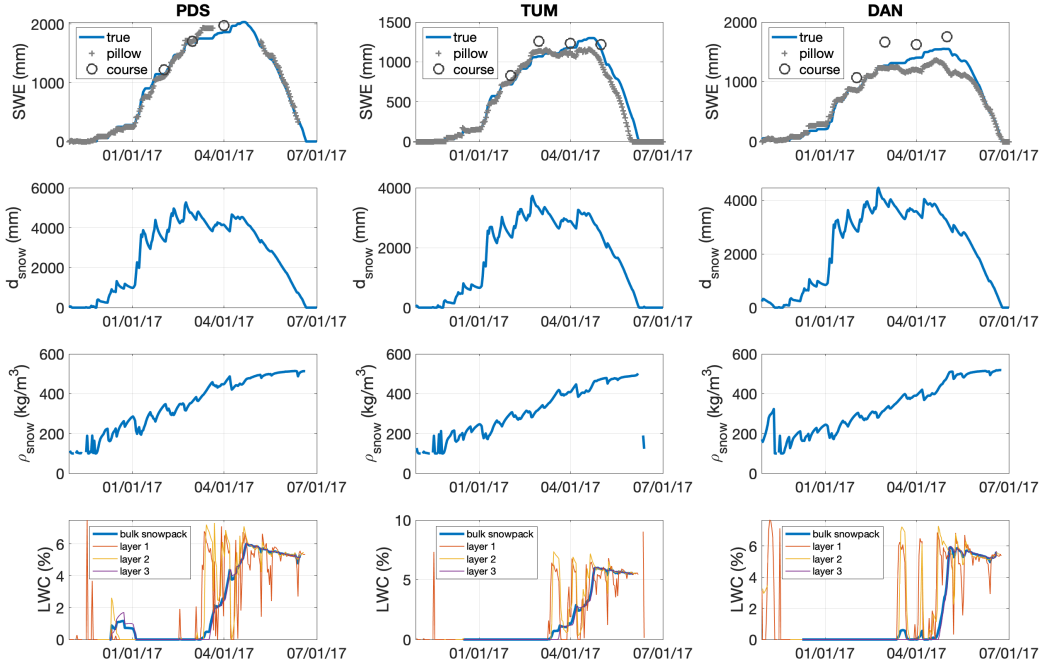

Figure 5. True (nature run) bulk snowpack states (blue curves) for the PDS (left column), TUM (middle column), and DAN (right column) sites. The rows respectively show SWE (first), snow depth (second), snow density (third) and LWC (fourth). The snowpack is discretized in up to three layers as shown for LWC for the top (orange, top 100 mm of snow depth), middle (gold, next 200 mm of snow depth), and bottom (purple; remaining snowpack depth) layers. The simulated true SWE (blue line, top panels) is compared to the in situ snow pillow and snow course data. The true SWE was calibrated to the in situ observations through adjustment of the precipitation bias correction factor (Eq. (6)) at each site.

The true unwrapped observable phase delay based on the 6-day sampling interval is shown in Fig. 6. Gaps in the measurement sequence result from either a mixed pair of dry and wet conditions in the snowpack or wet-wet snowpack pairs. The second row in Fig. 6 identifies what viable dry-snow pairs exist for each site as a function of wavelength. PDS (lowest elevation), has the most LWC of the three sites and thus has the fewest dry-snow pairs during the accumulation season. In particular, the period with significant LWC at PDS in December results in no dry-snow pairs during that time. For TUM and DAN, dry-snow pairs exist every 6 days from early December to early March. As the snow transitions from dry to wet, the gaps in measurement availability depends on site and on wavelength, where longer wavelengths can more easily penetrate mildly wet snow. C- and L-band exhibit wet-snow behavior at PDS and TUM from late-March through snow disappearance, where wet-snow behavior at DAN does not occur until late April.

https://doi.org/10.5194/egusphere-2026-1594
Preprint. Discussion started: 30 April 2026

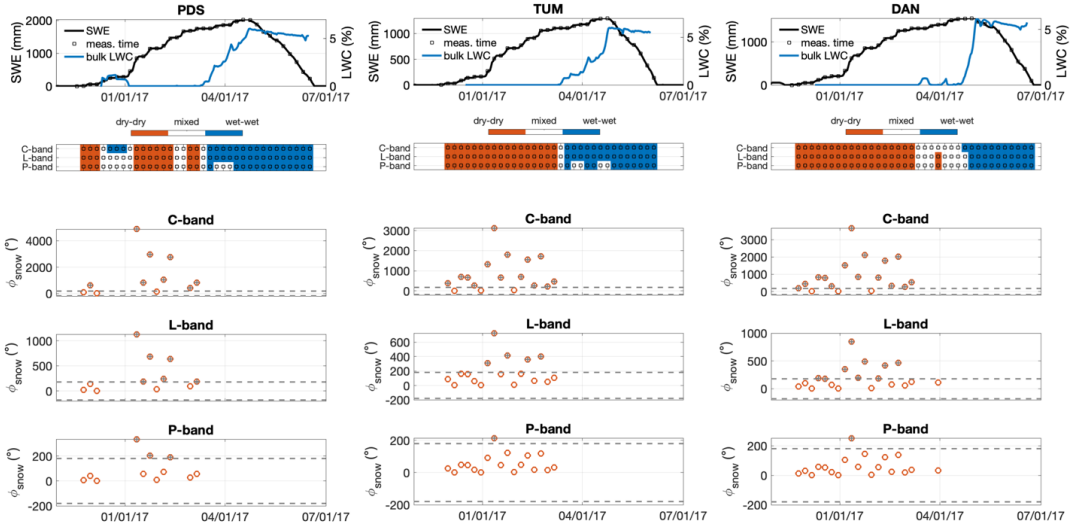

Figure 6. True unwrapped phase delay at C-, L-, and P-band at the PDS, TUM, and DAN sites. The top two rows show true SWE (black line) at the 6-day sampling frequency along with bulk LWC (blue line, mapped to right axis) and the diagnosed state of the snowpack as yielding viable dry-dry pairs vs. those that have mixed or wet-wet pairs. The bottom three rows show the true unwrapped phase delay corresponding to dry-dry pairs at each site. Any phase outside of the dashed grey lines (-180° - 180°, as indicated by the grey '+' symbol inside the open circle) would yield a wrapped measurement. In the OSSEs, these true phase delay values are corrupted by noise based on the specified measurement error standard deviation ($\boldsymbol{\sigma_{\phi_{snow}}}$).

The bottom three rows in Fig. 6 show the true unwrapped phase delay for each available measurement pair. Dry-snow pairs generally occur during the accumulation season and are associated with positive SWE changes leading to positive phase delays. DAN and TUM are idealized cases with no missing observations, because the snowpack is dry throughout the bulk of the accumulation season. Alternatively, PDS has measurement gaps during the accumulation season. Generally, the number of dry-snow observations goes up with elevation (drier snowpacks), where PDS, TUM, and DAN have 12, 17, and 18 available C-band observations respectively during the accumulation season. At DAN there is an extra measurement at both L- and P-band late in the accumulation season, where the limited LWC is insufficient to have phase delay deviate from the expected dry-snow behavior at those wavelengths. As expected, more measurements are subject to phase wrapping at shorter wavelengths. For example, at PDS, 8 of the 11 dry-snow true phase delay values would be wrapped at C-band, compared to 6 of 11 at L-band and only 3 of 11 at P-band. Additionally, for a measurement that would be wrapped, the number of wrapping cycles is highest at C-band and lowest at P-band.

4.2 OSSE results for phase delay measurement assimilation

4.2.1 Experiment #1: Assimilation of perfectly unwrapped phase measurements

Experiment #1 uses measurements of the pairwise phase delay, where, if corresponding to large enough SWE changes, the phase delay is perfectly unwrapped from the expected limits of (-180° to 180°) to unbounded values outside this range. Hence the phase delay measurements in this experiment are the same as the true unwrapped phase delay shown in Fig. 6, but with random measurement error added. The number of measurements that require unwrapping and the

https://doi.org/10.5194/egusphere-2026-1594
Preprint. Discussion started: 30 April 2026

number of cycles of wrapping per measurement are a strong function of frequency (Fig. 6). Perfect unwrapping therefore represents an optimistic end-member case that should closely correspond to the lower bound of estimation error, by removing all potential unwrapping errors.

Experiment #1 results with assimilation of phase measurements ($\phi_{snow,obs}$) at C-, L-, and P-band (with baseline measurement error $\sigma_{\phi_{snow}}$ = 20°) for the DAN site are shown in Fig. 7 for a single (random) measurement error instance. At DAN there is a phase measurement available every 6 days (Fig. 6). Fundamentally, the phase delay measurements provide information on dSWE between measurement times. The estimated dSWE for the deterministic retrieval and Bayesian approaches (relative to the true values) are shown in the left column of Fig. 7. The deterministic retrieval of dSWE (orange circles) performs well across all three frequencies, with negligible dSWE bias and dSWE RMSE of ~2 mm, 6 mm, and 20 mm for C-, L-, and P-band, respectively. The monotonic increase in RMSE with wavelength is a direct reflection of the fact that the phase delay is unwrapped and the signal-to-noise ratio is highest for C-band (i.e., unwrapped ϕ_{snow}~1000° as shown in Fig. 6 vs. $\sigma_{\phi_{snow}}$ = 20°) and lowest for P-band (i.e., unwrapped ϕ_{snow}~100° vs. $\sigma_{\phi_{snow}}$ = 20°). The retrieval RMSE is primarily due to the propagation of random measurement error realizations contained in $\phi_{snow,obs}$ to dSWE estimates through the inversion of Eq. (2). In this case the retrieval estimates of SWE (based on the cumulative sum of dSWE; Sect. 3.3.3) closely follow the true SWE (Fig. 7, right column, orange circles) for all frequencies. Note that due to reduced sensitivity to LWC in the snowpack, L-band and P-band have one more measurement than C-band closer to peak SWE.

The Experiment #1 Bayesian estimation of dSWE at DAN (Fig. 7, left panel, blue triangles) also performs well, with negligible bias, but with RMSE that is reduced relative to the deterministic retrieval RMSE. Since the phase delay measurements provided to the retrieval and Bayesian estimation algorithms are identical, this reduced dSWE error is a result of the additional prior information provided by the snow model and acknowledgment of the measurement error characteristics ($\sigma_{\phi_{snow}}$). In other words, the Bayesian approach conditions the dSWE estimates on $\phi_{snow,obs}$ (while considering the prior estimates and measurement error) rather than fitting $\phi_{snow,obs}$ exactly (as implicit in the retrieval). This general property of Bayesian methods means that measurement errors will typically not propagate directly to estimates, explaining the damped RMSE relative to the retrieval estimates. The Bayesian result also accurately estimates SWE (Fig. 7, right column, blue lines) due to the accurate information content in dSWE combined with prior SWE information. Another benefit of the Bayesian approach is the continuous estimates of both SWE and its uncertainty, which is not available from the retrieval algorithm. The posterior ensemble uncertainty is generally smallest for C-band and largest for P-band due to the higher signal-to-noise ratio for unwrapped C-band measurements described above. The use of a snow model in the Bayesian framework also allows for extrapolating to melt-season SWE estimates (when there are no dry-snow phase measurements).

To emphasize the impact of the information content in the phase delay measurements on updating the prior in the Bayesian approach, a deterministic open-loop SWE estimate (using prior mean inputs to the snow model) is also shown in Fig. 7 (right panel, purple line). The bias between the open-loop and true SWE is primarily the result of differences in the prior mean value of the precipitation bias correction that is provided to the modeling framework (1.8) vs the true (calibrated) value of 1.63. The particle filter used herein simultaneously estimates the precipitation bias correction parameter (b) during the assimilation of phase measurements. The prior distribution and posterior

https://doi.org/10.5194/egusphere-2026-1594
Preprint. Discussion started: 30 April 2026

distribution (after all measurements are assimilated) for *b* is shown in Fig. 8. For all three frequencies, the bias correction parameter estimate by the posterior distribution (both mean and uncertainty) is improved with a narrower distribution for C-band and wider distribution for P-band. Simultaneous estimation of the snow states and the precipitation bias correction is primarily responsible for the narrow uncertainty in SWE throughout the accumulation season (most notable for C-band). After the accumulation season, when no more dry-snow phase measurements are assimilated, the posterior estimate uncertainty grows (Fig. 7) due to uncertainty in snowmelt. By estimating SWE during the accumulation season, the posterior ablation season SWE estimate is still generally better than the open loop estimate.

https://doi.org/10.5194/egusphere-2026-1594
Preprint. Discussion started: 30 April 2026

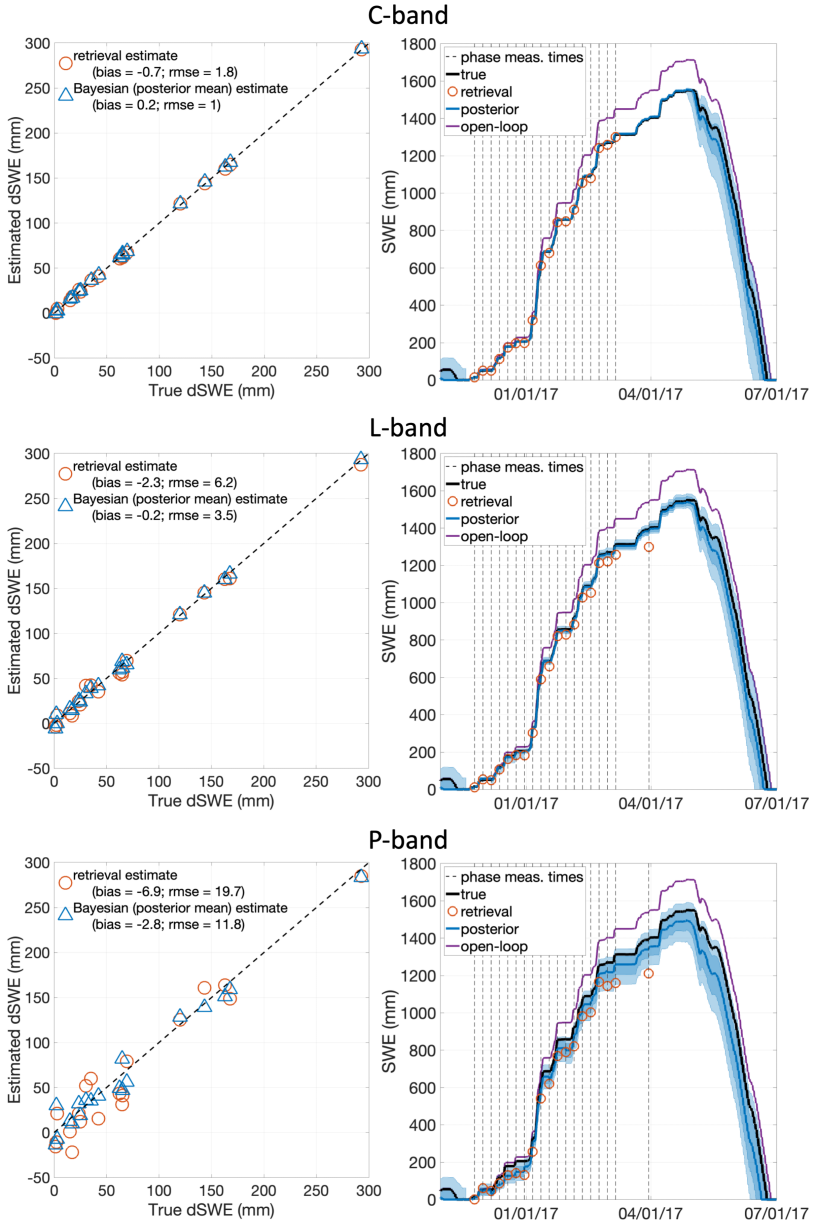

Figure 7. Experiment #1 (perfectly unwrapped phase delay) sample results for DAN with baseline phase measurement error $\sigma_{\phi_{snow}} = 20°$. (left column) Comparison of deterministic retrieval (orange circles) and Bayesian posterior (blue triangles) dSWE estimates vs. true dSWE values for: C-band (top), L-band (middle) and P-band (bottom). (right column) Comparison of absolute SWE estimates (retrieval as orange circles and posterior Bayesian as blue lines and shaded regions) and open-loop estimate (purple) vs. the true SWE (thick black line). The retrieved SWE is based on the accumulated dSWE retrieval estimates. The dark blue line represents the posterior median, the darker and lighter blue shaded region represents the posterior inter-quartile and 1st-99th percentile ranges respectively. The dashed vertical black lines are the times of available phase measurements (Fig. 6).

https://doi.org/10.5194/egusphere-2026-1594
Preprint. Discussion started: 30 April 2026

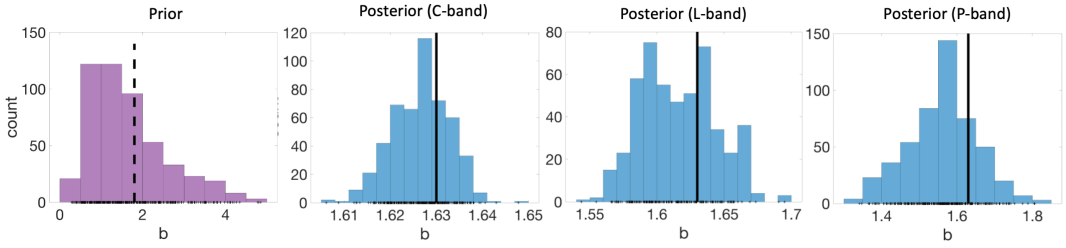

Figure 8. Open loop prior distribution (first column) and estimated posterior distributions of precipitation bias correction parameter ***b*** (after assimilation of all measurements) for C-band (second column), L-band (third column) and P-band (fourth column) measurements for the DAN results shown in Fig. 7. Black tick marks on x-axis represent individual particle values. The prior mean (1.8) is shown with the dashed line on the prior distribution and the true mean for DAN (1.63) is shown with the solid line on the posterior distributions.

Results for the estimation of dSWE and SWE at the PDS site are shown in Fig. 9 (the TUM results are not shown because they are similar to DAN). PDS is qualitatively different from DAN and TUM because of the additional temporal gap in phase measurements due to accumulation season LWC in the snowpack and the earlier onset of persistent LWC (Fig. 6), both of which lead to fewer phase measurements. In terms of dSWE estimates, both retrieval and Bayesian estimates again perform well at all three frequencies (Fig. 9, left column), with similar qualitative characteristics as seen in DAN – increasing RMSE in retrieval from C- through P-band, and damped dSWE RMSE in the Bayesian estimates vs. the retrieval estimates. The primary differences seen in the PDS results are in the SWE estimates, where the retrieval relies on reconstructing SWE from the cumulative sum of dSWE estimates, while the Bayesian approach has the additional information in the prior estimates of SWE when no observations are available. Specifically, the gap in phase measurements in December and early January misses several storms that generate dSWE during that period. For SWE estimates based on the deterministically retrieved dSWE values, there is no way to incorporate the "missing" dSWE values during that unmeasured period. The total amount of missing dSWE estimates directly propagates to the SWE estimates, leading to an underestimation across the rest of the accumulation season. This type of error could be mitigated by using existing in situ reference data to supplement retrieved dSWE, however in many regions such ancillary data does not exist. For the Bayesian estimates, the uncertainty during the unobserved period is relatively high, relying on prior dSWE and SWE estimates, but once measurements become available the information in the phase-dSWE relationship leads to more accurate SWE estimates. This is an important result highlighting that even where retrievals successfully estimate dSWE, temporal gaps between measurements can lead to significant errors in retrieved SWE. The use of a Bayesian approach can span those gaps with prior information, thus reducing SWE error.

https://doi.org/10.5194/egusphere-2026-1594
Preprint. Discussion started: 30 April 2026

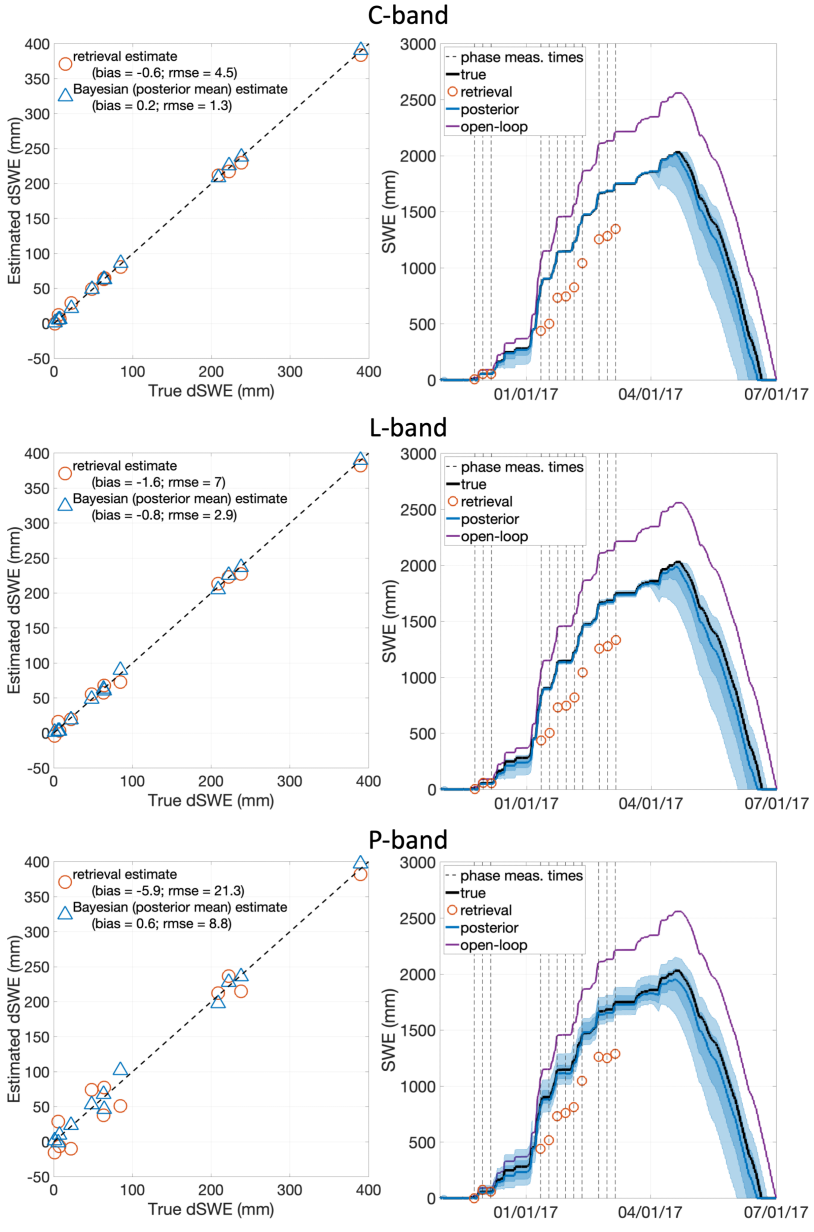

Figure 9. Same as Figure 7, but for PDS.

The sample results shown in Figs. 7 and 9 illustrate a single realization of synthetic measurement errors (i.e., a single randomly generated measurement error set with $\sigma_{\phi_{snow}}$ = 20°). To get more robust statistics, ten different realizations (each with $\sigma_{\phi_{snow}}$ = 20°) were run for each site. Figure 10 shows the error estimates for both dSWE and SWE when averaged across all realizations and all three sites. There is negligible dSWE bias in the retrieval and monotonically increasing dSWE RMSE as a function of frequency (from ~3 mm at C-band to ~23 mm at P-band).

https://doi.org/10.5194/egusphere-2026-1594
Preprint. Discussion started: 30 April 2026

The Bayesian dSWE RMSE estimates are smaller than the retrieval (by not fitting measurements exactly) with reductions in dSWE RMSE ranging between ~35-60%. The largest errors occur in using retrieved dSWE to estimate SWE, where the measurement gap at the PDS site introduces a negative SWE bias (~80 mm) across all three frequencies, which contributes significantly to the total SWE RMSE (~175 mm). The Bayesian estimates have SWE RMSE ranging from 9 mm at C-band to 61 mm at P-band, so that the Bayesian SWE RMSE is between ~5-34% of the deterministic retrieval RMSE values.

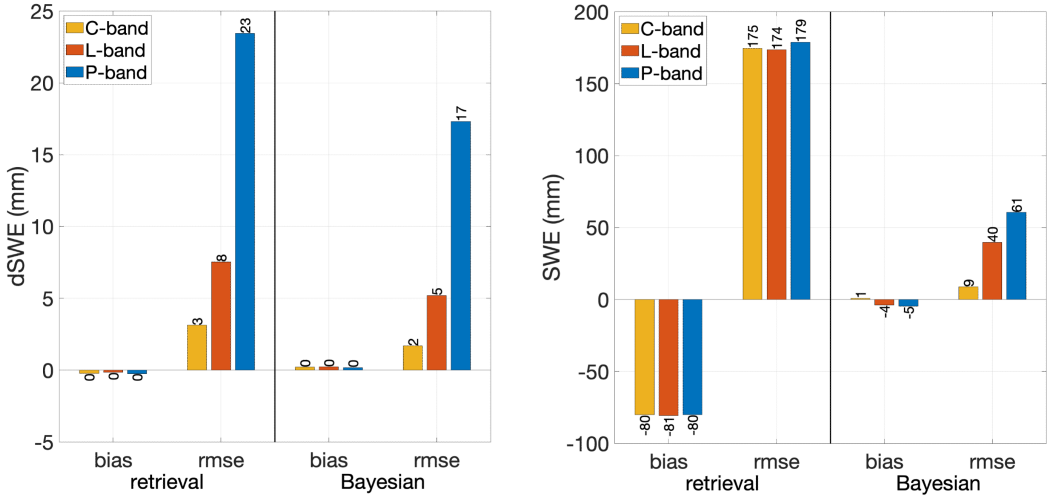

Figure 10. Experiment #1 (perfectly unwrapped phase delay) bias and RMSE for (left) dSWE estimation and (right) SWE estimation when averaged across all sites and synthetic measurement error realizations (with measurement error $\boldsymbol{\sigma_{\phi_{snow}}} = 20°$). The deterministic retrieval estimation errors are shown on the left of each panel, while the Bayesian estimation errors are shown on the right of each panel. Number labels are the bar height rounded to the nearest mm.

4.2.2 Discussion of Experiment #1 results

With no ambiguity with respect to phase unwrapping, the Experiment #1 results represent a lower bound of dSWE error for a given InSAR wavelength at the specified nominal phase delay measurement error ($\sigma_{\phi_{snow}} = 20°$). Estimation errors are expected to increase due to wrapping ambiguity, under higher measurement error, and with less frequent temporal revisit, which are explored in Experiment #2 and the sensitivity tests described below. Other aspects not explored herein include: time-varying measurement error and wavelength-dependent temporal decorrelation effects that will favor a higher number of measurements at longer wavelengths (Text S4). These time- and wavelength-dependent effects will lead to more variation in the quality of the dSWE estimates and will be best understood in the context of applications with real InSAR data. Even in the idealized conditions examined herein, where it is expected that the deterministic retrieval will perform well in dSWE estimation, it is demonstrated that the Bayesian framework can reduce propagation of random errors in $\phi_{snow,obs}$ to dSWE estimates through the acknowledgement of measurement error. Moreover, the Bayesian framework could handle the more complicated cases where there is time- and/or wavelength-dependent measurement error that can be derived as part of the phase delay retrieval process (Text S3) and built into the measurement model. It is also demonstrated that the prior information integral to the Bayesian

https://doi.org/10.5194/egusphere-2026-1594
Preprint. Discussion started: 30 April 2026

framework can mitigate errors in SWE estimation when there are significant temporal gaps in the measurement sequence (e.g., due to wet snow) that can "miss" dSWE events leading to poor reconstructed SWE from dSWE retrieval estimates alone.

4.2.3 Experiment #2: Assimilation of wrapped phase measurements

As illustrated in Fig. 6, the large SWE changes that occur at DAN, PDS, and TUM are consistent with a significant amount of expected phase wrapping across all three wavelengths examined. Experiment #2 uses the same set of pairwise measurements as Experiment #1, but with the phase delay wrapped between the measurable limits of -180° and 180°. These measurements are more representative of raw phase measurement where, without additional information, it would be unknown whether the phase has been wrapped or not. The use of wrapped phase for retrieval and assimilation represents another end-member case with the largest expected errors associated with wrapping ambiguity. For the retrieval approach, the wrapping ambiguity errors will propagate directly to dSWE and SWE estimates, while the Bayesian approach accounts for the inherent wrapping in the measurement model by using an appropriate likelihood function (Sect. 3.3.3).

The Experiment #2 dSWE and SWE estimates are again illustrated for a single measurement error realization at DAN in Fig. 11. In the scatter plots (left columns), the individual dSWE retrieval estimates based on wrapped phase measurements are marked with a '+' symbol inside the open circle for reference. The impact of wrapping is evident on the deterministically retrieved dSWE estimates, with a strong frequency dependence (Fig. 11, first column). For C-band, only three of the phase delay values are not wrapped at DAN. For measurements that are not wrapped (i.e., those with small enough dSWE values), the retrieved dSWE estimates are identical to the unwrapped case in Experiment #1. However, for the remaining wrapped measurements, C-band limits the range of retrieved dSWE to approximately +/- 25 mm. The true dSWE values for DAN (Fig. 11) range up to 300 mm (with five values above 100 mm). The overall retrieval errors are therefore large, with RMSE increasing from ~2 mm (Experiment #1, unwrapped) to ~104 mm (Experiment #2, wrapped) at DAN. For several measurements the sign of dSWE estimates is incorrect due to wrapping since, without prior information, negative phase is interpreted as a negative change in dSWE. Most of the bulk error is due to biases resulting from the wrapped dSWE retrievals. At L- and P-band, there are fewer wrapped observations, which mitigates the increased RMSE from Experiment #1 to Experiment #2: ~6 mm increasing to ~86 mm at L-band and ~20 mm increasing to ~99 mm at P-band. The larger dSWE retrieval errors propagate to SWE estimates, leading to significant underestimation for all three frequencies, with the smallest SWE errors occurring at P-band due to fewer wrapped measurements.

https://doi.org/10.5194/egusphere-2026-1594
Preprint. Discussion started: 30 April 2026

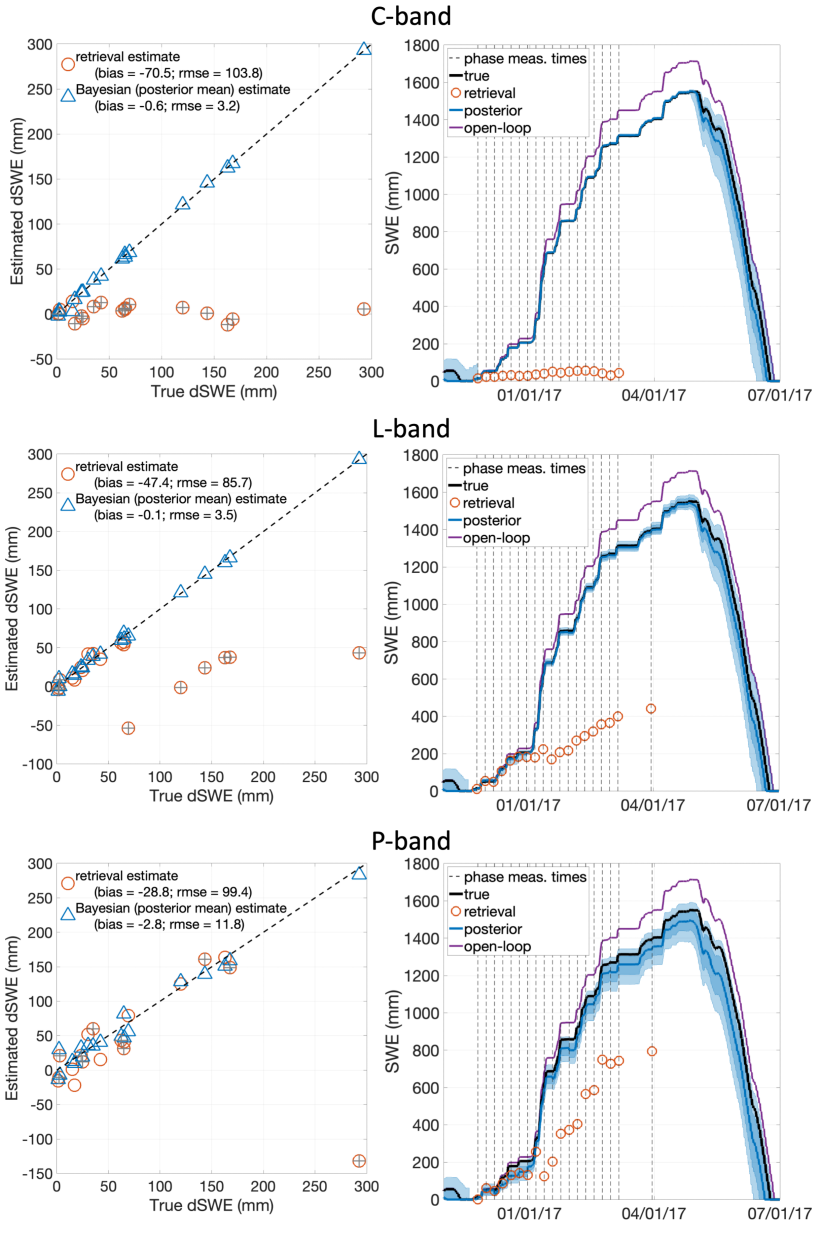

Figure 11. Same as Fig. 7 (DAN), but for Experiment #2 (wrapped phase delay). Retrieved dSWE values (left panel) that are based on wrapped phase measurements are marked with the grey '+' symbol inside the open circle. Without prior knowledge of wrapping, negative phase will be interpreted as negative dSWE values in the retrieval. The retrieved SWE is based on the accumulated dSWE retrieval estimates. SWE values below 0 mm are not shown.

At PDS (Fig. 12), the true dSWE values are larger than DAN, ranging up to 400 mm (with three values above 200 mm) and hence the errors associated with wrapping are larger. From Experiment #1 to Experiment #2, the retrieved dSWE RMSE increases from ~5 to 165 mm (C-band), ~7 to 173 mm (L-band) and ~21 to 244 mm (P-band)

https://doi.org/10.5194/egusphere-2026-1594
Preprint. Discussion started: 30 April 2026

580 across frequencies. The primary reason for the increase is the bias introduced when large true dSWE values lead to
581 wrapped phase, which is mitigated to some extent at longer wavelengths. These results illustrate the importance of
582 unwrapping algorithms in deterministic retrievals when applied to areas with large dSWE events.
583

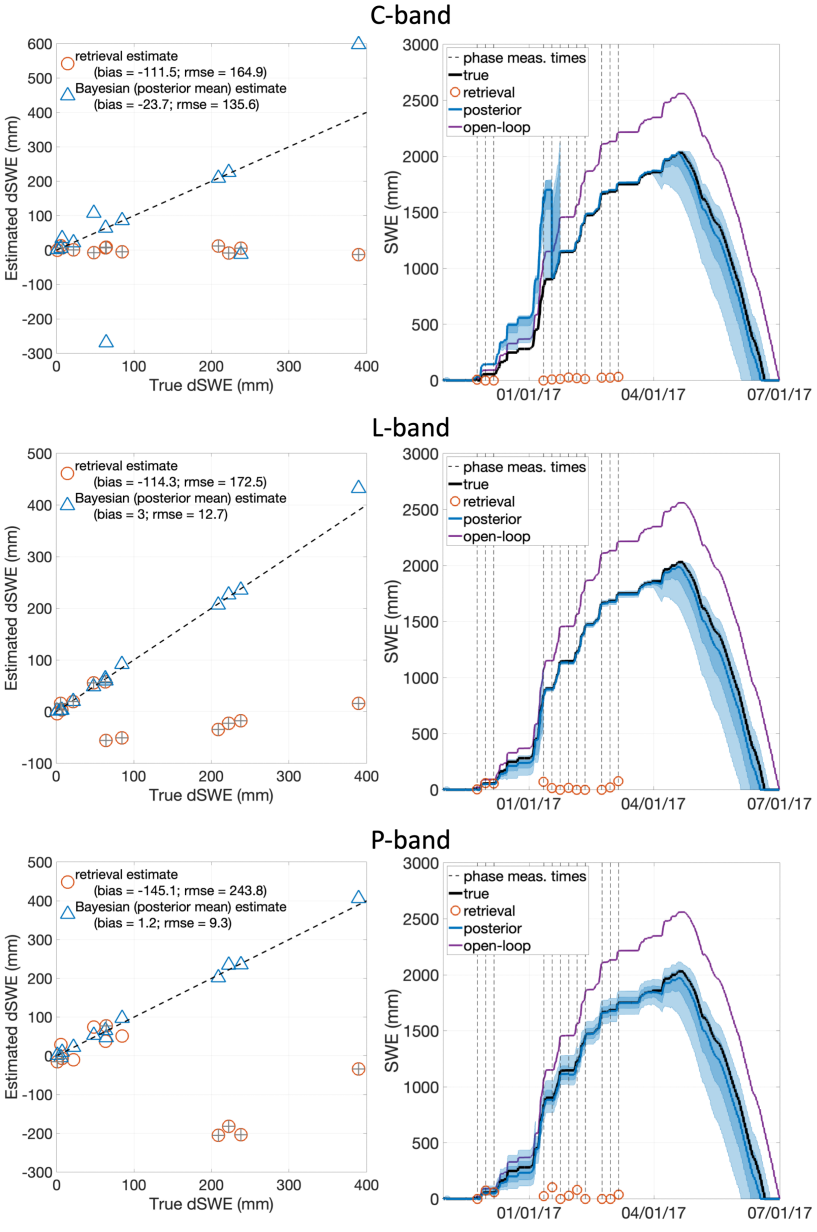

584

585 **Figure 12.** Same as Fig. 11, but for PDS.

https://doi.org/10.5194/egusphere-2026-1594
Preprint. Discussion started: 30 April 2026

The Bayesian estimation of dSWE at DAN (Fig. 11) shows the same RMSE for wrapped phase as unwrapped at L- and P-band, with only a minor increase (from ~1 mm to ~3 mm) at C-band. This is an important result that highlights that, with regular 6-day measurements, the ambiguity introduced by wrapping can be accounted for within the Bayesian approach using the wrapped Gaussian measurement error likelihood. At PDS (Fig. 12) there is more wrapping-induced degradation due to fewer measurements. With longer measurement gaps, especially early in the accumulation season, more prior dSWE uncertainty will accumulate leading to higher wrapping ambiguity. This is most noticeable at C-band, where the dSWE RMSE increases significantly from Experiment #1 to #2 (~1 mm to ~136 mm), because of the early-season measurement gap. This is seen in the top right panel of Fig. 12, where the Bayesian SWE estimate via assimilation of C-band phase delay has high uncertainty and significantly overestimates the true SWE before early February. The lack of measurements between December and mid-January lead to a positively biased precipitation bias correction parameter (b) and SWE that is not corrected until later in the season when more measurements become available. During that early season measurement gap, dSWE spans many C-band phase wrapping cycles, leading to higher ambiguity in the estimates at PDS relative to DAN. However, at L- and P-band, where wrapping cycles span larger dSWE values, the increase in dSWE RMSE when assimilating wrapped phase (relative to perfectly unwrapped) is much more modest: ~3 mm increasing to ~13 mm at L-band and less than 1 mm difference at P-band. While wrapping errors still directly propagate to the retrieved dSWE, in the Bayesian approach the prior dSWE values provide a constraint on likely values so that large errors will tend to occur only when the prior ensemble dSWE values occur over a wide enough range to span many wrapping cycles (most likely at C-band).

The Experiment #2 bulk estimation errors across all sites and ten measurement error realizations are shown in Fig. 13 and are consistent with the single-realization results shown above. The deterministic retrieval has largest dSWE bias at C-band and lowest at P-band due to fewer wrapping cycles at the longer wavelength. However, the larger signal-to-noise ratio for C-band (seen in Experiment #1) will generally reduce the random errors compared to those at longer wavelengths (Fig. 10). These competing factors result in total retrieved dSWE RMSE that is more uniform across wavelengths (~120-140 mm) in the wrapped phase case. The larger biases in retrieved dSWE estimates at C-band propagate to SWE so that the retrieval SWE estimates are more accurate (lower bias and RMSE) at L- and P-band when using wrapped phase. The Bayesian estimates of dSWE and SWE are much more accurate (nearly unbiased at L- and P-band) with better performance at L- and P-band compared to C-band. The Bayesian performance at C-band is good when 6-day measurements are available during the accumulation season (i.e., at DAN and TUM), but degrade significantly when there are measurement gaps due to wet snow (i.e., at PDS). During early season measurement gaps, the precipitation bias correction factor can be poorly estimated and constrained, leading to large dSWE uncertainty and phase wrapping at C-band, leading to large errors in Bayesian dSWE and SWE estimates.

https://doi.org/10.5194/egusphere-2026-1594
Preprint. Discussion started: 30 April 2026

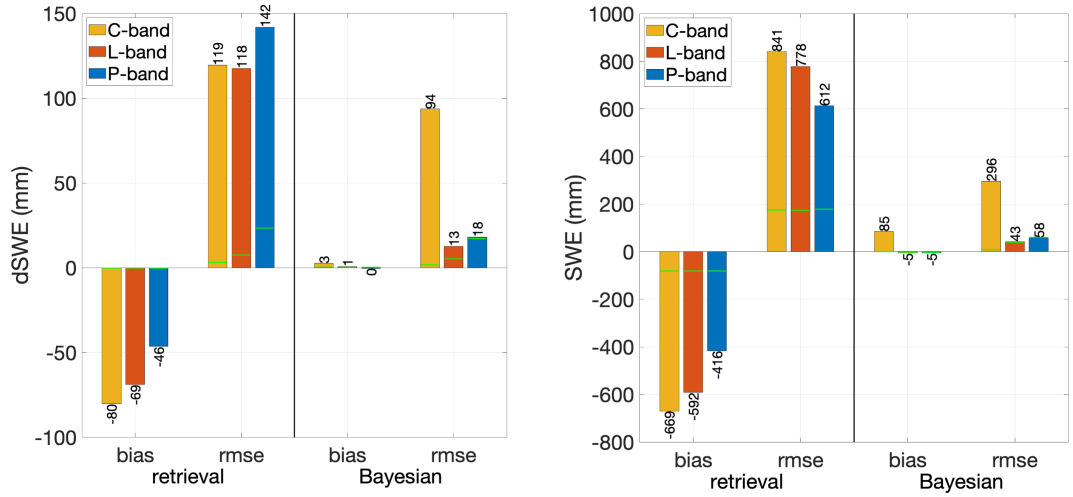

Figure 13. Same as Fig. 10 but for Experiment #2 (wrapped phase). The green horizontal lines for each bar are the Experiment #1 error estimates (shown in Fig. 10) provided as a reference.

4.2.4 Discussion of Experiment #2 results

The Experiment #2 results represent a pessimistic end-member case where there is full ambiguity related to phase wrapping. The deterministic retrieval approach generally relies on an accurate unwrapping of phase delay and is therefore not expected to do well in this case where many measurements are wrapped. Application of unwrapping algorithms (Sect. 2.2.2) will generally both mitigate some of these errors and introduce additional error, likely leading to results somewhere between the Experiment #1 (perfect unwrapping) and Experiment #2 (no unwrapping) results. The Bayesian framework is shown to be able to perform reasonably well at dSWE estimation (and significantly better than the deterministic retrieval) under the stringent conditions of using only unwrapped phase by taking the ambiguity in measurement error with wrapped phase into account. This is most true at L- and P-band where the wrapping is both less common and wrapped phase is over fewer wrapping cycles. For cases where there are significant temporal gaps in the measurement sequence (i.e. at PDS) that can lead to large a priori dSWE uncertainty. The large number of wrapping cycles at C-band introduces more ambiguity than at L- and P-band, leading to the largest dSWE and SWE estimation bias and RMSE. At C-band (and at PDS) in particular, wrapping ambiguity cannot be fully disentangled in the Bayesian approach leading to large dSWE biases (~85 mm) that are much smaller at L- and P-band (~ 5 mm). This propagates to SWE estimates where C-band SWE RMSE is ~6 times larger than at L- or P-band (Fig. 13).

4.3 Sensitivity to phase measurement error standard deviation and repeat-pass frequency

4.3.1 Impact of phase measurement error

To assess the sensitivity of the results to bulk measurement error, Experiment #1 and #2 were repeated for phase measurement error standard deviations of $\sigma_{\phi_{snow}}$ = 10°, 40°, and 60°. Fig. 14 shows the Experiment #1 (perfectly unwrapped) results for the different measurement error standard deviation cases tested (averaged over ten measurement error realizations). For the retrieval of dSWE, the bias is small across all frequencies and the RMSE

https://doi.org/10.5194/egusphere-2026-1594
Preprint. Discussion started: 30 April 2026

increases monotonically with measurement error as expected (Eq. (2)). The random errors are smallest for C-band (ranging from 3-6 mm) and largest for P-band (12-70 mm) based on their relative signal-to-noise ratios. When perfectly unwrapped, the tested measurement errors are still relatively small compared to the phase delay corresponding to the large dSWE values. In estimating SWE from the deterministically retrieved dSWE values, RMSE is dominated by large biases at all frequencies due to measurement gaps at PDS (Fig. 6) such that there is limited dependence of retrieval SWE RMSE on $\sigma_{\phi_{snow}}$. The Bayesian dSWE estimates are unbiased with smaller RMSE than the retrieval RMSE across all frequencies and measurement error values. The Bayesian SWE estimates do not suffer from the same biases due to missing dSWE associated with measurement gaps and are significantly smaller than the retrieved estimates of SWE as a result. The Bayesian SWE RMSE as a function of measurement error standard deviation ranges from 4-11 mm for C-band, 23-57 mm for L-band, and 36-136 mm for P-band.

Figure 15 shows the Experiment #2 (wrapped phase) results, which demonstrate that the deterministic retrieval errors are dominated by wrapping ambiguity errors with limited dependence on measurement error standard deviation. These large wrapping errors propagate to the retrieved estimates of SWE, which are very large (600-800 mm). The largest Bayesian estimation error occurs at C-band, where wrapping ambiguity led to large errors at PDS due to early-season measurement gaps resulting from wet snow. Overall, the Bayesian estimates are more robust to phase wrapping errors, and therefore dSWE and SWE errors are smaller and do show some dependence on measurement error standard deviation compared to the retrieval estimates. Across the range of examined measurement error standard deviations, the SWE RMSE as a function of wavelength ranges from 195-400 mm (C-band), 25-232 mm (L-band), and 35-213 mm (P-band).

https://doi.org/10.5194/egusphere-2026-1594
Preprint. Discussion started: 30 April 2026

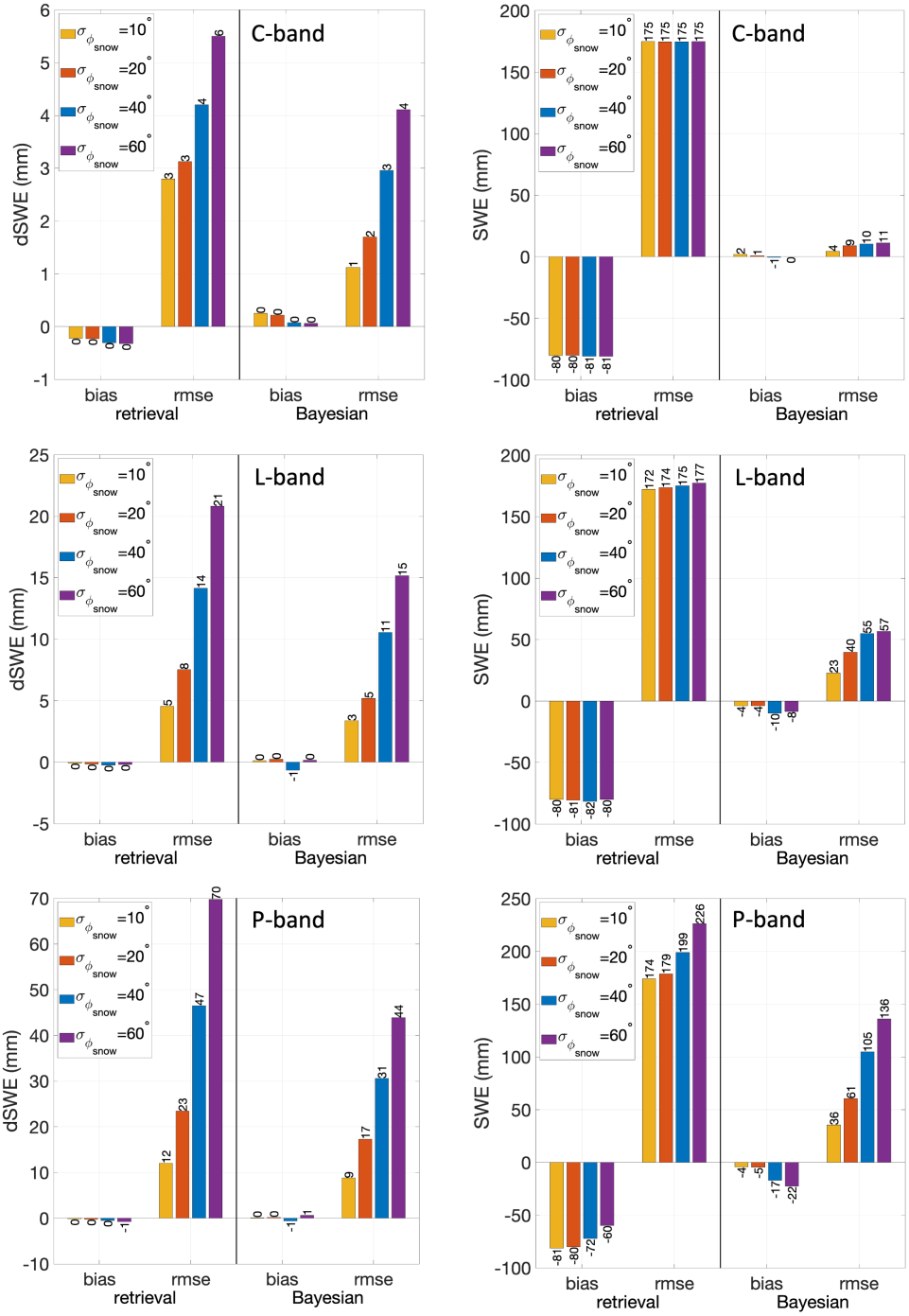

Figure 14. (top row) Experiment #1 (unwrapped phase delay) dSWE and SWE estimation bias and RMSE vs. measurement error standard deviation with C-band measurements. (middle row) Same as top row but for L-band. (bottom row) Same as top row but for P-band. Number labels are the bar height rounded to the nearest mm.

https://doi.org/10.5194/egusphere-2026-1594
Preprint. Discussion started: 30 April 2026

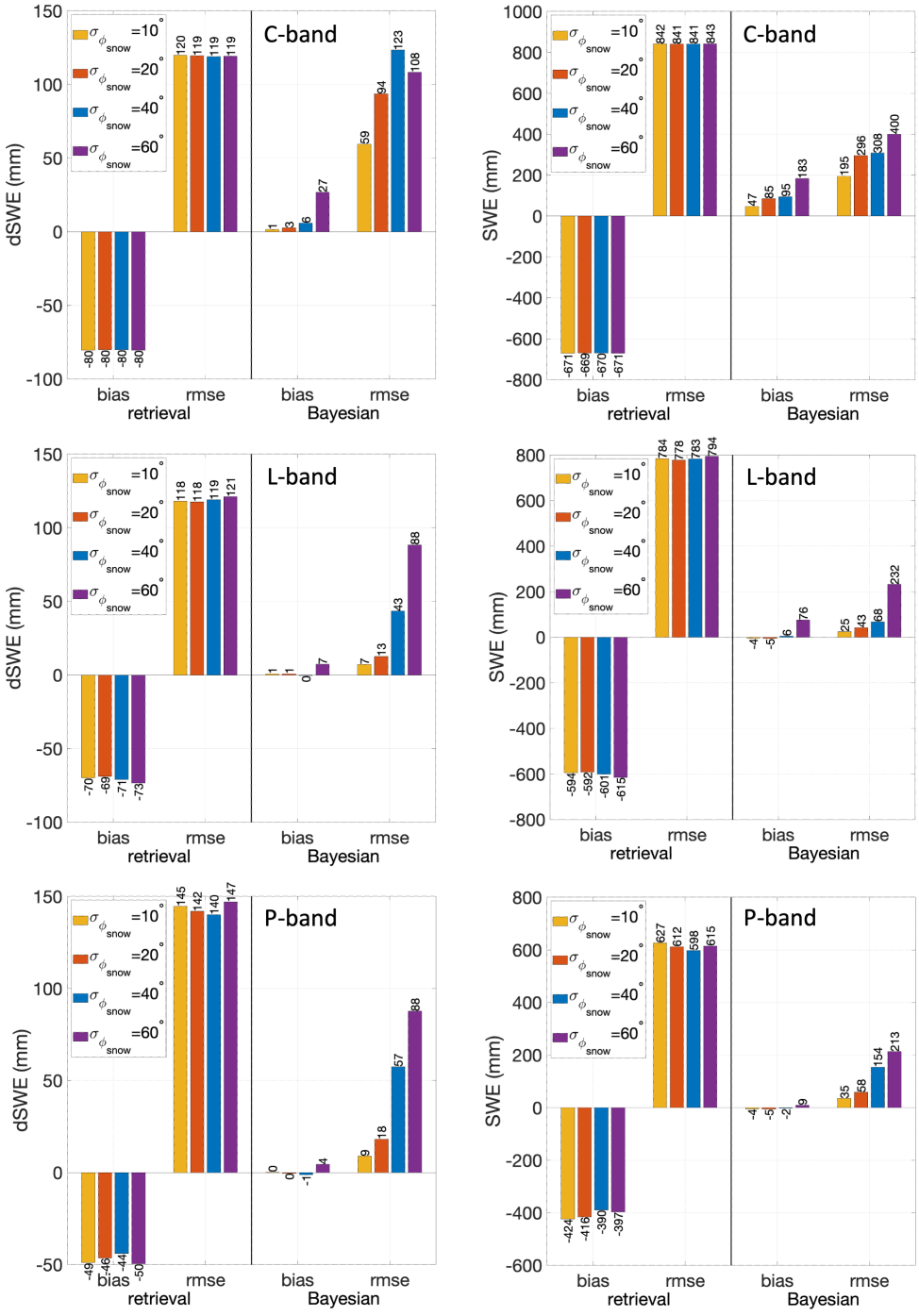

Figure 15. Same as Fig. 14, but for Experiment #2 (wrapped phase delay).

https://doi.org/10.5194/egusphere-2026-1594
Preprint. Discussion started: 30 April 2026

4.3.2 Impact of decreasing repeat pass frequency from 6 to 12 days

To assess the sensitivity of the results to measurement sampling frequency, Experiment #1 and #2 were repeated for a 12-day repeat pass. All other baseline parameters were held the same, including the baseline measurement error standard deviation ($\sigma_{\phi_{snow}}$ = 20°) and the temporal decorrelation rule (i.e., decorrelation only beyond 12 days). The 12-day repeat frequency corresponds to normal operations for NISAR and Sentinel-1 or ROSE-L with a single satellite (Table 1). In the 12-day sampling experiments, the number of dry-snow measurements is identical for all three frequencies with 6, 9, and 9 measurements at PDS, TUM, and DAN, respectively. The primary differences relative to the 6-day configuration are that: (1) there are fewer measurements, making individual random measurement errors more impactful on performance and (2) a generally larger dSWE between pairwise measurements. This latter factor has two competing implications. The larger dSWE will provide a stronger signal in phase change. So, for the same measurement error there will be a larger signal-to-noise ratio. This has the potential to improve individual dSWE estimates, especially at P-band where the natural signal-to-noise ratio is smaller than C-band. However, the larger dSWE values also serve to increase the likelihood of wrapping and potential for wrapping errors in Experiment #2. The increase in wrapping will happen at all frequencies, but will be most evident at C-band.

Figure 16 shows the bulk estimation error characteristics for all stations for both unwrapped and wrapped 12-day phase delay measurements. For Experiment #1 (Fig. 16, top row), the retrieval estimates for dSWE at the 12-day repeat are comparable to the baseline (6-day). L-band dSWE RMSE is essentially unchanged, while C-band RMSE increases slightly and P-band RMSE decreases slightly. In constructing retrieved estimates of SWE from the accumulated 12-day dSWE retrievals, the bias and RMSE increase slightly at all frequencies. The bias in retrieved SWE estimates is still largely due to the same measurement gap at PDS in the early accumulation season which misses dSWE (snowfall) events. For the Bayesian estimates, there are only small variations relative to the 6-day estimates, with slight improvements in both dSWE and SWE RMSE at L- and P-band, due to larger signal-to-noise ratios.

For the Experiment #2 12-day results (Fig. 16, bottom row), the retrieval dSWE and SWE errors are large and increase significantly relative to the baseline (6-day) results. Specifically, the dSWE bias nearly doubles and contributes significantly to the RMSE. This is explained by the larger number of wrapped measurements (due to larger dSWE changes over 12 vs. 6 days) that ultimately bias the dSWE estimates and then propagate to SWE. The Experiment #2 Bayesian estimates of dSWE and SWE at a 12-day repeat show an increase in RMSE at C-band and L-band. The dSWE RMSE is smallest at P-band (~16 mm), which is least susceptible to wrapping error, while the SWE estimates are comparable at L- and P-band to each other and to the baseline 6-day repeat results (~54 mm).

https://doi.org/10.5194/egusphere-2026-1594
Preprint. Discussion started: 30 April 2026

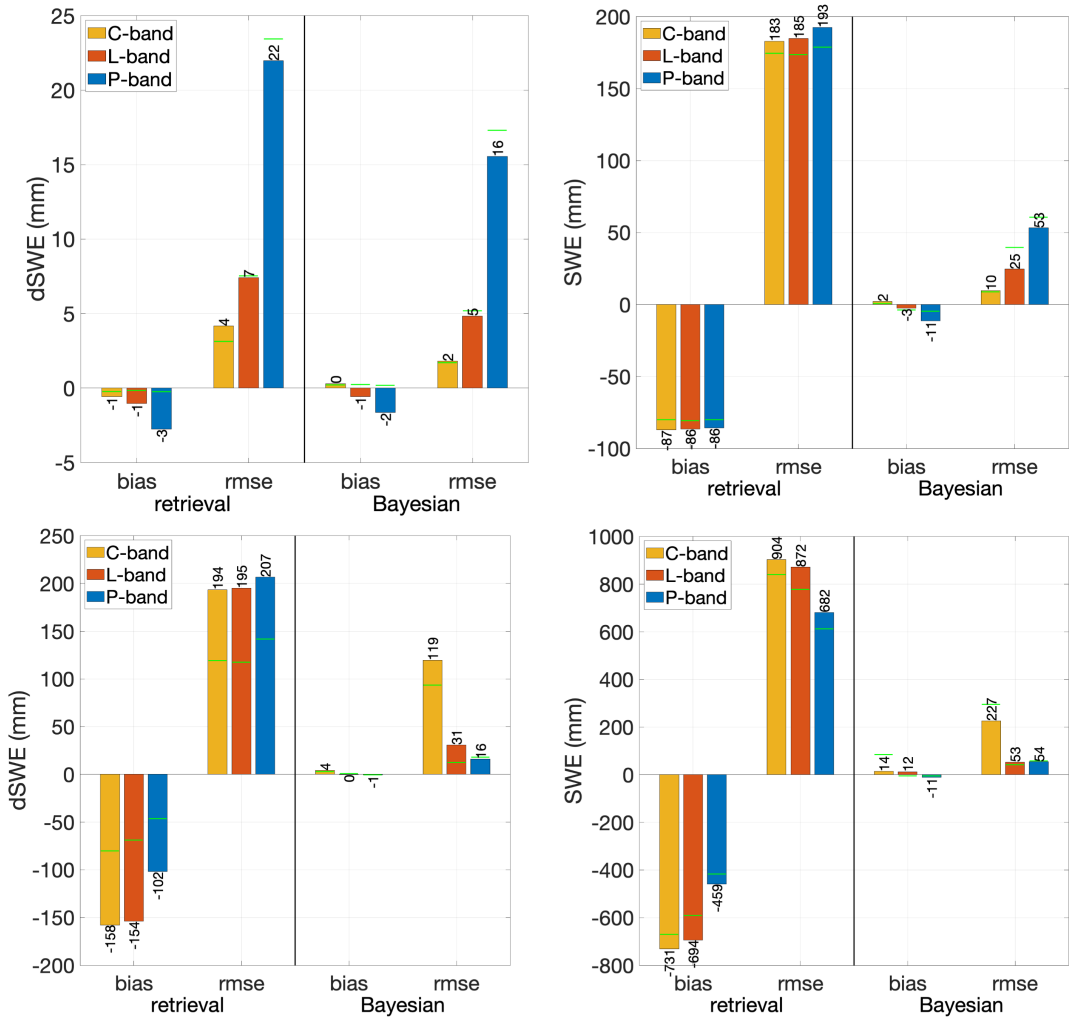

Figure 16. (top row) Experiment #1 (unwrapped phase) bias and RMSE for 12-day repeat for (left column) dSWE estimation and (right column) SWE estimation when averaged across all three sites. The green horizontal reference lines for each bar are the Experiment #1 (unwrapped, 6-day) error estimates provided as a reference. (bottom row) Same as top row, but for Experiment #2 (wrapped phase). The green horizontal reference lines for each bar are the Experiment #2 (wrapped, 6-day) error estimates provided as a reference. Number labels are the bar height rounded to the nearest mm.

https://doi.org/10.5194/egusphere-2026-1594
Preprint. Discussion started: 30 April 2026

4.3.3 Discussion of sensitivity test results

The sensitivity tests spanning measurement error standard deviation ($\sigma_{\phi_{snow}}$) show qualitatively similar results to the baseline experiments. Experiment #1 (perfectly unwrapped phase) shows unbiased dSWE estimates for both the retrieval and Bayesian approaches with increasing dSWE RMSE as a function of $\sigma_{\phi_{snow}}$. The Bayesian dSWE RMSE is generally damped relative to the deterministic retrieval, where random measurement error is propagated directly to the dSWE estimates. The reconstruction of SWE from retrieval dSWE estimates, generally leads to large bias (underestimation) due to temporal gaps in measurements, while the Bayesian SWE RMSE is significantly less. For Experiment #2 (wrapped phase), the ambiguity in phase introduces large errors in the retrieval estimates of dSWE and the resulting reconstruction of SWE. The Bayesian approach has largely unbiased estimates for dSWE and SWE at L- and P-band, but the larger ambiguity (i.e., across many more wrapping cycles) at C-band introduces larger bias in both dSWE and SWE (albeit lower than the retrieval estimates) across all measurement error values.

The sensitivity test using a 12-day repeat highlights the presence of more potential signal (i.e., higher dSWE) over 12 vs. 6 days, but with a concurrent increase in wrapping ambiguity. As such, Experiment #1 (unwrapped phase) 12-day results have negligible degradation in dSWE at C-band and improvements at L- and P-band, with similar relative performance in SWE estimation for both retrieval and Bayesian estimates. For Experiment #2 (wrapped phase), the retrieval errors in dSWE nearly double in bias, which contributes to significant dSWE RMSE and SWE error estimates. The 12-day dSWE results are best for P-band (due to the increased signal-to-noise ratio), with L- and C-band dSWE RMSE about a factor of ~2 and ~7 larger respectively than the 6-day results. It should be noted that in these experiments simple temporal decorrelation rules were used such that all frequencies had available measurements at the 12-day repeat pass. At 12-day repeat, it is expected that C-band measurements could become less available, that P-band would be most available, and with the number of available L-band measurements in between.

5. Conclusions

This work has presented a Bayesian InSAR phase data assimilation framework for estimating dSWE and SWE from phase delay measurements at C-, L-, and P-band. The framework was tested using a set of OSSEs applied to a deep snow year at sites in the Tuolumne watershed where dSWE (snowfall) events are large. The Bayesian estimates are compared to deterministic retrieval estimates and open-loop modeling estimates. A baseline experiment with a 6-day repeat frequency and 20° phase delay measurement error standard deviation was examined along with sensitivity to variations in measurement error and increase in temporal repeat frequency.

The Bayesian approach benefits significantly from both prior information (i.e., snow model estimates) and the acknowledgement and specification of measurement error to generally outperform the retrieval approach in both estimation of dSWE and SWE. In the end-member case of perfectly unwrapped phase measurements, the deterministic retrieval works well

https://doi.org/10.5194/egusphere-2026-1594
Preprint. Discussion started: 30 April 2026

in estimation of dSWE (lowest error at C-band and highest at P-band). Missing measurements at all frequencies due to snow wetness, but most likely at C-band, result in missing dSWE events that leads to significant errors in reconstructed SWE. This is emblematic of the need for auxiliary SWE reference data to aid retrievals in propagating dSWE estimates to SWE estimates. The Bayesian approach for the perfectly unwrapped case performs better than retrieval with reduced dSWE RMSE. Estimation of SWE is also significantly better in the Bayesian case since prior model estimates of SWE between missing measurements account for first-order estimates of unobserved dSWE events.

In the end-member case of fully wrapped phase measurements, ambiguity due to wrapping leads to very large (bias) errors in deterministically retrieved dSWE. This is somewhat mitigated at L- and P-band, which span a larger dSWE range across a wrapping cycle, but even those estimates are affected by the large dSWE cases examined herein. Real applications that attempt to first unwrap phase delay measurements will likely fall between these two end-member cases. However, unwrapping algorithms perform best with prior information on SWE changes, which are not generally available. In the wrapped phase experiment, the Bayesian framework accounts for wrapping within the measurement error model that, when combined with the prior information provided by the modeling framework, yields estimates comparable to the perfectly unwrapped case. This is true at all frequencies, even though C-band experiences significant wrapping for the large dSWE values at the experimental sites. The exception to this was with C-band phase delay at PDS where a significant temporal measurement gap early in the season (i.e., due to wet snow) did not constrain the large uncertainty in the precipitation bias correction parameter and in dSWE, causing significant wrapping ambiguity that is not easily corrected. Additionally, in both experiments, the Bayesian approach shows promise as a value-added approach to estimating SWE from phase delay measurements that are not only accurate at the measurement times, but interpolate between measurements (i.e., across snow wetness events) and extrapolate beyond measurements (i.e., into melt season), and provide distributional (uncertainty) estimates for dSWE and SWE.

Several caveats should be mentioned and considered in future work: The OSSEs performed herein are idealized (flat terrain, constant measurement error, etc.) and tests should be extended to spatially distributed cases that span a large range of variations in elevation, slope/aspect, forest cover, snowpack wetness, and other relevant physiographic, snow, and soil characteristics. The general performance should be confirmed with real phase data (e.g., using Sentinel-1 C-band and NISAR L-band data along with existing airborne and tower-based datasets) in environments where collocated SWE verification data exists to understand how more realistic error sources and ambiguity due to wrapping may impact results. Specific areas in need of further examination include: (1) using real data to identify realistic temporal decorrelation seen in C-, L, or P-band phase delay, (2) assessing and testing more realistic phase measurement errors that will vary with frequency and in space/time, (3) understanding the impact of wrapping, including when using unwrapping algorithms, and (4) examining estimation performance in more complex conditions (e.g., complex terrain with forest cover).

https://doi.org/10.5194/egusphere-2026-1594
Preprint. Discussion started: 30 April 2026

Supplement link

See Supplemental Information.

Author contributions

SM, XX, MG, HM, RS, ED, SY, DE, and JL contributed to the conceptualization of the overarching ideas and goals of the work. SM designed and carried out the experiments, and performed the analysis. SM prepared the manuscript draft with contributions to the final version from all co-authors.

Competing interests

The authors declare that they have no conflict of interest.

Disclaimer

Copernicus Publications remains neutral with regard to jurisdictional claims made in the text, published maps, institutional affiliations, or any other geographical representation in this paper. While Copernicus Publications makes every effort to include appropriate place names, the final responsibility lies with the authors. Views expressed in the text are those of the authors and do not necessarily reflect the views of the publisher.

Acknowledgements

The authors acknowledge Jeff Dozier who provided valuable insight into many of the ideas behind this work.

Financial support

This work was supported by NASA Terrestrial Hydrology Program (THP) grant #80NSSC25M7047 and the NASA FINESST grant #80NSSC24K0022.

References

Agiomyrgiannakis, Y. and Stylianou, Y.: Wrapped Gaussian Mixture Models for Modeling and High-Rate Quantization of Phase Data of Speech. *IEEE Trans. Audio Speech Lang. Process.*, 17(4), 775–786, https://doi.org/10.1109/TASL.2008.2008229, 2009.

https://doi.org/10.5194/egusphere-2026-1594
Preprint. Discussion started: 30 April 2026

Alonso-Gonzalez, E., Gutmann, E., Aalstad, K., Fayad, A., Bouchet, M., and Gascoin, S.: Snowpack dynamics in the Lebanese mountains from quasi-dynamically downscaled ERA5 reanalysis updated by assimilating remotely sensed fractional snow-covered area. *Hydrol. Earth Syst. Sci.*, 25, 4455–4471, https://doi.org/10.5194/hess-25-4455-2021, 2021.

Alonso-Gonzalez, E., Lopez-Moreno, J. I., Gascoin, S., García-Valdecasas Ojed, M., Sanmiguel-Vallelado, A., Navarro-Serrano, F., Revuelto, J., Ceballos, A., Esteban-Parr, M. J., and Essery, R.: Daily gridded datasets of snow depth and snow water equivalent for the Iberian Peninsula from 1980 to 2014. *Earth Syst. Sci. Data*, 10, 303–315, https://doi.org/10.5194/essd-10-303-2018, 2018.

Arulampalam, M. S., Maskell, S., Gordon, N., and Clapp, T.: A Tutorial on Particle Filters for Online Nonlinear/Non-Gaussian Bayesian Tracking, *IEEE Trans. Signal Process.*, **50**, 174–188, https://doi.org/10.1109/78.978374, 2002.

Chang, A. T. C., Foster, J. L., and Hall, D. K.: Nimbus-7 SMMR derived global snow cover parameters. *Ann. Glaciol.*, 9, 39–44, 1987.

Chen, C. W. and Zebker, H. A.: Network approaches to two dimensional phase unwrapping: Intractability and two new algorithms. *J. Opt. Soc. Am. A*, 17, 401–414, https://doi.org/10.1364/JOSAA.17.000401, 2000.

Cho, E., Vuyovich, C. M., Kumar, S. V., Wrzesien, M. L., and Kim, R. S.: Evaluating the Utility of Active Microwave Observations as a Snow Mission Concept Using Observing System Simulation Experiments. *The Cryosphere Discuss.*, 1–24, https://doi.org/10.5194/tc-2022-211, 2022.

Conde, V., Nico, G., Mateus, P., Catalão, J., Kontu, A., and Gritsevich, M.: On The Estimation of Temporal Changes of Snow Water Equivalent by Spaceborne Sar Interferometry: A New Application for the Sentinel-1 Mission. *J. Hydrol. Hydromech.*, 67, 93–100, https://doi.org/10.2478/johh-2018-0003, 2019.

Costantini, M., Farina, A., and Zirilli, F.: A fast phase unwrapping algorithm for SAR interferometry. *IEEE Trans. GARS*, 37(1), 452–460, https://doi.org/10.1109/36.736365, 1999.

Davidson, G. W. and Bamler, R.: Multiresolution Phase Unwrapping for SAR Interferometry. *IEEE Trans. Geosci. Remote Sens.*, 37, 163–174, https://doi.org/10.1109/36.739151, 1999.

Davidson, M., Furnell, R., Geudtner, D., Gebert, N., Petrolati, D., Iannini, L., Osborne, S., and Thales Alenia Space: Copernicus ROSE-L SAR mission. In *Proceedings of the 14th European Conference on Synthetic Aperture Radar (EUSAR 2022)* (pp. 1–4), VDE Verlag, https://doi.org/10.1109/IGARSS47720.2021.9554018, 2022.

Deeb, E. J., Forster, R. R., and Kane, D. L.: Monitoring Snowpack Evolution Using Interferometric Synthetic Aperture Radar on the North Slope of Alaska, USA. *Int. J. Remote Sens.*, 32, 3985–4003, https://doi.org/10.1080/01431161003801351, 2011.

DeLannoy, G., Reichle, R., Houser, P., Arsenault, K., Verhoest, N., and Pauwels, V.: Satellite-scale snow water equivalent assimilation into a high-resolution land surface model. *J. Hydrometeor.*, 11, 352–369, https://doi.org/10.1175/2009JHM1192.1, 2010.

https://doi.org/10.5194/egusphere-2026-1594
Preprint. Discussion started: 30 April 2026

Derksen, C., Lemmetyinen, J., King, J., Belair, S., Garnaud, C., Lapointe, M., Crevier, Y., Burbidge, G., and Siqueira, P.: A Dual-Frequency Ku-Band RADAR Mission Concept for Seasonal Snow. In *IGARSS 2019-2019 IEEE International Geoscience and Remote Sensing Symposium* (pp. 5742–5744), https://doi.org/10.1109/IGARSS.2019.8906663, 2019.

Dozier, J., Bair, E. H., and Davis, R. E.: Estimating the spatial distribution of snow water equivalent in the world's mountains. *WIREs Water*, 3, 461–474, https://doi.org/10.1002/wat2.1140, 2016.

Durand, M. and Margulis, S. A.: Feasibility test of multifrequency radiometric data assimilation to estimate snow water equivalent. *J. Hydrometeorol.*, 7(3), 443–457, https://doi.org/10.1175/JHM498.1, 2006.

Durand, M. and Margulis, S. A.: Correcting first-order errors in snow water equivalent estimates using a multifrequency, multiscale radiometric data assimilation scheme. *J. Geophys. Res.*, 112, D13121, https://doi.org/10.1029/2006JD008067, 2007.

Essery, R.: A factorial snowpack model (FSM 1). *Geosci. Model Dev.*, 8, 3867–3876, https://doi.org/10.5194/gmd-8-3867-2015, 2015.

Essery, R., Morin, S., Lejeune, Y., and Menard, C.: A comparison of 1701 snow models using observations from an alpine site. *Adv. Water Resour.*, 55, 131–148, https://doi.org/10.1016/j.advwatres.2012.07.013, 2013.

Fang, Y., Liu, Y., Li, D., Sun, H., and Margulis, S. A.: Spatiotemporal snow water storage uncertainty in the midlatitude American Cordillera. *The Cryosphere*, 17, 5175–5195, https://doi.org/10.5194/tc-17-5175-2023, 2023.

Fang, Y., Liu, Y., and Margulis, S. A.: A western United States snow reanalysis dataset over the Landsat era from water years 1985 to 2021. *Sci. Data*, 9, 763, https://doi.org/10.1038/s41597-022-01768-7, 2022.

Farr, T. G., Rosen, P. A., Caro, E., Crippen, R., Duren, R., Hensley, S., … and Alshoufi, Y.: The Shuttle Radar Topography Mission. *Rev. Geophys.*, 45, https://doi.org/10.1029/2005RG000183, 2007.

Flynn, T. J.: Two-dimensional phase unwrapping with minimum weighted discontinuities. *J. Opt. Soc. Am. A*, 14, 2692–2701, https://doi.org/10.1364/JOSAA.14.002692, 1997.

Fornaro, G., Franceschetti, G., and Lanari, R.: Interferometric SAR Phase unwrapping using Green's formulation. *IEEE Trans. GARS*, 34(3), 720–727, https://doi.org/10.1109/36.495034, 1996.

Garnaud, C., Derksen, C., King, J., Walker, A., Lemmetyinen, J., and Bélair, S.: Quantifying Snow Mass Mission Concept Trade-Offs Using an Observing System Simulation Experiment. *J. Hydrometeorol.*, 20(1), 155–173, https://doi.org/10.1175/JHM-D-17-0241.1, 2019.

Gascoin, S., Luojus, K., Nagler, T., Lievens, H., Masiokas, M., Jonas, T., … and De Rosnay, P.: Remote sensing of mountain snow from space: status and recommendations. *Front. Earth Sci.*, 12, 1381323, 2024.

Gelaro, R., McCarty, W., Suárez, M. J., Todling, R., Molod, A., Takacs, L., … and Zhao, B.: The Modern-Era Retrospective Analysis for Research and Applications, Version 2 (MERRA-2). *J. Clim.*, 30, 5419–5454, https://doi.org/10.1175/JCLI-D-16-0758.1, 2017.

Ghiglia, D. C. and Romero, L. A.: Minimum Lp-norm two-dimensional phase unwrapping. *J. Opt. Soc. Am. A*, 13(10), 1–15, https://doi.org/10.1364/JOSAA.13.001999, 1996.

https://doi.org/10.5194/egusphere-2026-1594
Preprint. Discussion started: 30 April 2026

Girotto, M., Margulis, S. A., and Durand, M.: Probabilistic SWE reanalysis as a generalization of deterministic SWE reconstruction techniques. *Hydrol. Process.*, 28(12), 3875–3895, 2014.

Goldstein, R. M., Zebker, H. A., and Werner, C. L.: Satellite Radar Interferometry: Two-dimensional Phase Unwrapping. *Radio Sci.*, 23, 713–720, https://doi.org/10.1029/RS023i004p00713, 1988.

Guenther, D., Marke, T., Essery, R., and Strasser, U.: Uncertainties in snowpack simulations—Assessing the impact of model structure, parameter choice, and forcing data error on point-scale energy balance snow model performance. *Water Resour. Res.*, 55, 2779–2800, https://doi.org/10.1029/2018WR023403, 2019.

Guneriussen, T., Hogda, K., Johnsen, H., and Lauknes, I.: In-SAR for Estimation of Changes in Snow Water Equivalent of Dry Snow. *IEEE Trans. Geosci. Remote*, 39, 2101–2108, https://doi.org/10.1109/36.957273, 2001.

Hale, K., Meyer, J., Tarricone, J., Vuyovich, C., Mason, M., Marshall, H.-P., et al.: What's next for snow: Insights from the NASA terrestrial hydrology program community snow meeting. *Earth's Future*, 13, e2025EF006460, https://doi.org/10.1029/2025EF006460, 2025.

Hoppinen, Z., Oveisgharan, S., Marshall, H.-P., Mower, R., Elder, K., and Vuyovich, C.: Snow water equivalent retrieval over Idaho – Part 2: Using L-band UAVSAR repeat-pass interferometry. *The Cryosphere*, 18, 575–592, https://doi.org/10.5194/tc-18-575-2024, 2024.

Hoppinen, Z., Palomaki, R. T., Marshall, H.-P., et al.: Separating Snow from Signal: Quantifying Non-Snow Errors in InSAR SWE Retrievals. *TechRxiv*, https://doi.org/10.36227/techrxiv.175433198.81344547/v1, 2025.

Immerzeel, W. W., van der Meer, G. H., and de Haas, A.: Importance and vulnerability of the world's water towers. *Nature*, 577(7790), 364–369, https://doi.org/10.1038/s41586-019-1822-y, 2020.

Jeong, J., Tsang, L., Xu, X., Yueh, S., and Margulis, S. A.: Full-Wave Electromagnetic Model Simulations of P-Band Radio Signal Propagation Through Forest Using the Fast Hybrid Method. *IEEE J. Sel. Top. Appl. Earth Obs. Remote Sens.*, 16, 1–12, https://doi.org/10.1109/JSTARS.2023.3292324, 2023.

Krinner, G., Derksen, C., Essery, R., Fahnestock, M., and Lejeune, Y.: ESM-SnowMIP: assessing snow models and quantifying snow-related climate feedbacks. *Geosci. Model Dev.*, 11, 5027–5049, https://doi.org/10.5194/gmd-11-5027-2018, 2018.

Kumar, G., Date, P., Pachori, R. B., Swaminathan, R., and Singh, A. K.: Wrapped Particle Filtering for Angular Data. *IEEE Access*, 10, 90287–90298, https://doi.org/10.1109/ACCESS.2022.3200478, 2022.

Kuptametee, C., and Aunsri, N.: A review of resampling techniques in particle filtering framework. *Measurement*, 193, https://doi.org/10.1016/j.measurement.2022.110836, 2022.

Leinss, S., Wiesmann, A., Lemmetyinen, J., and Hajnsek, I.: Snow Water Equivalent of Dry Snow Measured by Differential Interferometry. *IEEE J. Sel. Top. Appl. Earth Obs. Remote Sens.*, 8(8), 3773–3790, https://doi.org/10.1109/JSTARS.2015.2432031, 2015.

https://doi.org/10.5194/egusphere-2026-1594
Preprint. Discussion started: 30 April 2026

Lettenmaier, D. P., Alsdorf, D., Dozier, J., Huffman, G. J., Pan, M., and Wood, E. F.: Inroads of remote sensing into hydrologic science during the WRR era. *Water Resour. Res.*, 51, 7309–7342, https://doi.org/10.1002/2015WR017616, 2015.

Li, H., Wang, Z., He, G., and Man, W.: Estimating Snow Depth and Snow Water Equivalence Using Repeat-Pass Interferometric SAR in the Northern Piedmont Region of the Tianshan Mountains. *J. Sensors*, 2017, 1–17, https://doi.org/10.1155/2017/8739598, 2017.

Liu, J. and West, M.: Combined Parameter and State Estimation in Simulation-Based Filtering, in: Sequential Monte Carlo Methods in Practice, edited by: Doucet, A., de Freitas, N., and Gordon, N., Statistics for Engineering and Information Science, Springer, New York, NY, 197–223, https://doi.org/10.1007/978-1-4757-3437-9_10, 2001.

Luojus, K., Pulliainen, J., Metsämäki, S., Cohen, J., and Lemmetyinen, J.: GlobSnow v3.0 Northern Hemisphere snow water equivalent dataset. *Sci. Data*, 8(1), 163, https://doi.org/10.1038/s41597-021-00939-2, 2021.

Magnusson, J., Wever, N., Essery, R., Helbig, N., Winstral, A., and Jonas, T.: Evaluating snow models with varying process representations for hydrological applications. *Water Resour. Res.*, 51, 2707–2723, https://doi.org/10.1002/2014WR016498, 2015.

Mankin, J. S., Viviroli, D., Singh, D., Hoekstra, A. Y., and Diffenbaugh, N. S.: The potential for snow to supply human water demand in the present and future. *Environ. Res. Lett.*, 10, https://doi.org/10.1088/1748-9326/10/11/114016, 2015.

Margulis, S.A., Girotto, M., Cortés, G. and Durand, M.:: A Particle Batch Smoother Approach to Snow Water Equivalent Estimation, *J. Hydrometeor.*, 16, 1752-1772, https://doi.org/10.1175/JHM-D-14-0177.1, 2015.

Margulis, S. A., Liu, Y., and Baldo, E.: A Joint Landsat- and MODIS-Based Reanalysis Approach for Midlatitude Montane Seasonal Snow Characterization, *Front. Earth Sci.*, **7**, 272, https://doi.org/10.3389/feart.2019.00272, 2019.

Masutani, M., and Coauthors: Observation System Simulation Experiments. In W. A. Lahoz, B. Khattatov, and R. Ménard (Eds.), *Data Assimilation*, 647–677, Springer, https://doi.org/10.1007/978-3-540-71045-8_25, 2010.

Mazzotti, G., Essery, R., Moeser, C. D., and Jonas, T.: Resolving small-scale forest snow patterns using an energy balance snow model with a one-layer canopy. *Water Resour. Res.*, 56, https://doi.org/10.1029/2019WR026129, 2020a.

Mazzotti, G., Essery, R., Webster, C., Malle, J., and Jonas, T.: Process-level evaluation of a hyper-resolution forest snow model using distributed multisensory observations. *Water Resour. Res.*, 56, https://doi.org/10.1029/2020WR027572, 2020b.

Mazzotti, G., Webster, C., Essery, R., and Jonas, T.: Increasing the physical representation of forest-snow processes in coarse-resolution models: Lessons learned from upscaling hyper-resolution simulations. *Water Resour. Res.*, 57, https://doi.org/10.1029/2020WR029064, 2021.

Mazzotti, G., Webster, C., Queno, L., Cluzet, B., and Jonas, T.: Canopy structure, topography, and weather are equally important drivers of small-scale snow cover dynamics in sub-alpine forests. *Hydrol. Earth Syst. Sci.*, 27, 2099–2121, https://doi.org/10.5194/hess-27-2099-2023, 2023.

https://doi.org/10.5194/egusphere-2026-1594
Preprint. Discussion started: 30 April 2026

Metsämäki, S., Anttila, K., Vepsäläinen, J., and Pulliainen, J.: Introduction to GlobSnow Snow Extent products with considerations for accuracy assessment. *Remote Sens. Environ.*, 156, 96–108, https://doi.org/10.1016/j.rse.2014.09.018, 2015.

Moradkhani, H., Hsu, K.-L., Gupta, H., and Sorooshian, S.: Uncertainty assessment of hydrologic model states and parameters: Sequential data assimilation using the particle filter, Water Resour. Res., **41**, W05012, https://doi.org/10.1029/2004WR003604, 2005.

Mott, R., Winstral, A., Cluzet, B., Helbig, N., Magnusson, J., Mazzotti, G., Queno, L., Schirmer, M., Webster, C., and Jonas, T.: Operational snow-hydrological modelling for Switzerland. *Front. Earth Sci.*, 11, 1228158, https://doi.org/10.3389/feart.2023.1228158, 2023.

Nagler, T., Rott, H., Hetzenecker, M., Wuite, J., and Potin, P.: The Sentinel 1 Mission: New Opportunities for Ice Sheet Observations. *Remote Sens.*, 7(7), 9371–9389, https://doi.org/10.3390/rs70709371, 2015.

Nagler, T., Rott, H., Scheiblauer, S., Libert, L., Mölg, N., Horn, R., Fischer, J., Keller, M., Moreira, A., and Kubanek, J.: Airborne Experiment on Insar Snow Mass Retrieval in Alpine Environment. In *IGARSS 2022 – 2022 IEEE International Geoscience and Remote Sensing Symposium*, 4549–4552, https://doi.org/10.1109/IGARSS46834.2022.9883809, 2022.

NASA: Shuttle Radar Topography Mission (SRTM). https://www2.jpl.nasa.gov/srtm/, 2013.

National Academies of Sciences, Engineering, and Medicine (NASEM): Thriving on Our Changing Planet: A Decadal Strategy for Earth Observation from Space. *The National Academies Press*, https://doi.org/10.17226/24938, 2018.

Oveisgharan, S., Zinke, R., Hoppinen, Z., and Marshall, H.-P.: Snow water equivalent retrieval over Idaho – Part 1: Using Sentinel-1 repeat-pass interferometry. *The Cryosphere*, 18, 559–574, https://doi.org/10.5194/tc-18-559-2024, 2024.

Pritchard, D. M. W., Forsythe, N., O'Donnell, G., Fowler, H. J., and Rutter, N.: Multi-physics ensemble snow modelling in the western Himalaya. *The Cryosphere*, 14, 1225–1244, https://doi.org/10.5194/tc-14-1225-2020, 2020.

Qin, Y., Waha, K., Vanuytrecht, E., and Liu, Y.: Agricultural risks from changing snowmelt. *Nat. Clim. Change*, 10, 459–465, https://doi.org/10.1038/s41558-020-0746-8, 2020.

Roe, G. H.: Orographic precipitation. *Annu. Rev. Earth Planet. Sci.*, 33(1), 645–671, https://doi.org/10.1146/annurev.earth.33.092203.122541, 2005.

Rosen, P., Hensley, S., Shaffer, S., Edelstein, W., Kim, Y., Kumar, R., Misra, T., Bhan, R., and Sagi, R.: The NASA-ISRO SAR (NISAR) Mission Dual-Band Radar Instrument Preliminary Design. In *2017 IEEE International Geoscience and Remote Sensing Symposium (IGARSS)*, 3832–3835, https://doi.org/10.1109/IGARSS.2017.8127836, 2017.

Rott, H., Nagler, T., and Scheiber, R.: Snow Mass Retrieval by Means of SAR Interferometry. In *FRINGE '03 Workshop: Advances in SAR Interferometry from ERS and ENVISAT Missions*, 1–6, 2003.

Rott, H., Yueh, S., Cline, D. W., Duguay, C., Essery, R., Haas, C., Hélière, F., Kern, M., Macelloni, G., Malnes, E., Nagler, T., Pulliainen, J., Rebhan, H., and Thompson, A.: Cold Regions Hydrology High-resolution Observatory for Snow and Cold Land Processes. *Proc. IEEE*, 98(5), 752–765, https://doi.org/10.1109/JPROC.2009.2038947, 2010.

https://doi.org/10.5194/egusphere-2026-1594
Preprint. Discussion started: 30 April 2026

Ruiz, J. J., et al.: Investigation of environmental effects on coherence loss in SAR interferometry for snow water equivalent retrieval. *IEEE Trans. Geosci. Remote Sens.*, 60, 1–15, https://doi.org/10.1109/TGRS.2022.3223760, 2022.

Shrestha, P., and Barros, A. B.: Assimilation of L-band interferometric synthetic aperture radar (InSAR) snow depth retrievals for improved snowpack quantification. *The Cryosphere*, 19, 2895–2911, https://doi.org/10.5194/tc-19-2895-2025, 2025.

Siirila-Woodburn, E. R., Rhoades, A. M., Hatchett, B. J., Huning, L. S., Szinai, J., Tague, C., … and Kaatz, L.: A low-to-no snow future and its impacts on water resources in the western United States. *Nat. Rev. Earth Environ.*, 2(11), 800–819, 2021.

Takala, M., Luojus, K., Pulliainen, J., and Metsämäki, S.: Estimating northern hemisphere snow water equivalent for climate research through assimilation of space-borne radiometer data and ground-based measurements. *Remote Sens. Environ.*, 115(12), 3517–3529, https://doi.org/10.1016/j.rse.2011.08.014, 2011.

Tarricone, J., Webb, R. W., Marshall, H.-P., Nolin, A. W., and Meyer, F. J.: Estimating snow accumulation and ablation with L-band interferometric synthetic aperture radar (InSAR). *The Cryosphere*, 17, 1997–2019, https://doi.org/10.5194/tc-17-1997-2023, 2023.

Tsang, L., Xu, X., Yueh, S. H., Oveisgharan, S., Hoppinen, Z., and Marshall, H.-P.: Review article: Global monitoring of snow water equivalent using high-frequency radar remote sensing. *The Cryosphere*, 16(9), 3531–3573, https://doi.org/10.5194/tc-16-3531-2022, 2022.

Wrzesien, M.L., Pavelsky, T.M., Durand, M.T., Dozier, J., and Lundquist, J.D.: Characterizing Biases in Mountain Snow Accumulation From Global Data Sets, *Water Resources Research,* 55(11), 9873-9891, https://doi.org/10.1029/2019WR025350, 2019.

Wu, Y.-Y. and Madson, A.: Error Sources of Interferometric Synthetic Aperture Radar Satellites, Remote Sens., **16**, 354, https://doi.org/10.3390/rs16020354, 2024.

Yueh, S., Dinardo, S., Akgiray, A., West, R., Cline, D., Elder, K: Airborne Ku-Band Polarimetric Radar Remote Sensing of Terrestrial Snow Cover, *IEEE Trans. Geosci. Remote Sens.,* 47, 3347 – 3364, https://doi/org/10.1109/TGRS.2009.2022945, 2009.

Yueh, S., Xu, X., Shah, R., Kim, Y., Garrison, J., Komanduru, A., and Elder, K.: Remote Sensing of Snow Water Equivalent Using Coherent Reflection From Satellite Signals of Opportunity: Theoretical Modeling, *IEEE J. Sel. Top. Appl. Earth Obs. Remote Sens.*, 10, 1–12, https://doi.org/10.1109/JSTARS.2017.2743172, 2017.

Yueh, S. H., Shah, R., Xu, X., Stiles, B., and Bosch-Lluis, X.: A Satellite Synthetic Aperture Radar Concept Using P-Band Signals of Opportunity, *IEEE J. Sel. Top. Appl. Earth Obs. Remote Sens.*, **14**, 2796–2816, https://doi.org/10.1109/JSTARS.2021.3059242, 2021.